GSK3B-mediated phosphorylation of MCL1 regulates axonal autophagy to promote Wallerian degeneration

Shuji Wakatsuki, Shinji Tokunaga, Megumi Shibata, and Toshiyuki Araki

Department of Peripheral Nervous System Research, National Institute of Neuroscience, National Center of Neurology and Psychiatry, 4-1-1 Ogawa-higashi, Kodaira, Tokyo 187-8502, Japan

Macroautophagy is a catabolic process, in which portions of cytoplasm or organelles are delivered to lysosomes for degradation. Emerging evidence has indicated a pathological connection between axonal degeneration and autophagy. However, the physiological function and induction mechanism of autophagy in axons remain elusive. We herein show that, through activation of BECLIN1, glycogen synthase kinase 3B (GSK3B)–mediated phosphorylation of BCL2 family member MCL1 induces axonal autophagy and axonal degeneration. Phosphorylated MCL1 is ubiquitinated by the FBXW7 ubiquitin ligase and degraded by the proteasome, thereby releasing BECLIN1 to induce axonal autophagy. Axonal autophagy contributes to local adenosine triphosphate production in degenerating axons and the exposure of phosphatidylserine—an "eat-me" signal for phagocytes—on transected axons and is required for normal recruitment of phagocytes to axonal debris in vivo. These results suggest that GSK3B–MCL1 signaling to regulate autophagy might be important for the successful completion of Wallerian degeneration.

Introduction

Axonal degeneration is recognized as a key pathological feature of many neurological disorders, including Alzheimer's disease and Parkinson's disease (Wang et al., 2012; Conforti et al., 2014). A typical form of pathological axonal degeneration is Wallerian degeneration, which has been observed in segments distal to the site of injury. We previously reported a ubiquitin proteasome system (UPS)–regulated signaling mechanism with the ability to regulate axonal integrity during Wallerian degeneration (Wakatsuki et al., 2011, 2015). Upon the initiation of Wallerian degeneration, the ubiquitin ligase zinc and ring finger 1 (ZNRF1) targets AKT for degradation via the UPS. Glycogen synthase kinase 3B (GSK3B), which is activated by the loss of AKT-mediated phosphorylation, phosphorylates and inactivates collapsin response mediator protein 2 (CRMP2) to induce its degradation. The degradation of CRMP2 leads to the loss of cytoskeletal integrity, which promotes Wallerian degeneration. These findings indicate that GSK3B is one of the critical mediators regulating Wallerian degeneration.

Autophagy is a primary homeostatic pathway through which a portion of the cytoplasm is engulfed by autophagosomes and delivered to lysosomes for its degradation (Yang and Klionsky, 2010; Shen and Mizushima, 2014). Autophagy is a highly regulated process that is typically induced by nutrient starvation or stress (Lum et al., 2005; Yamamoto and Yue, 2014). Autophagy has also been implicated in the regulation of axonal degeneration: an increase in autophagy markers and the formation of autophagosomes has been reported in degenerating axons (Yang et al., 2013; Wong and Holzbaur, 2015). However, the pathophysiological significance and regulation of axonal autophagy remain elusive.

We herein provide a novel role for autophagy in axonal degeneration. Using Wallerian degeneration models in vitro and in vivo, we demonstrate that the BCL2 family protein MCL1 negatively regulates axonal autophagy by binding to BECLIN1, a key regulator of autophagy, and also that the GSK3B-mediated phosphorylation of MCL1 serves as an initiating signal to induce axonal autophagy. Phosphorylated MCL1 was ubiquitinated by FBXW7 ubiquitin ligase and degraded through the UPS, which accelerated Wallerian degeneration. The perturbation of axonal autophagy affected the exposure of phosphatidylserine (PS), an "eat-me" signal for phagocytes, on transected axons, resulting in the decreased recruitment of phagocytic cells to axonal debris in vivo. These results have identified the regulatory mechanism of axonal autophagy through the GSK3B–MCL1 pathway as a molecular basis for Wallerian degeneration.

Correspondence to Shuji Wakatsuki: swaka@ncnp.go.jp; or Toshiyuki Araki: taraki@ncnp.go.jp

Abbreviations used: DRG, dorsal root ganglia; DTAF, 5-([4,6-dichlorotriazinyl] amino)fluorescein; GSK3B, glycogen synthase kinase 3B; MMP, mitochondrial membrane potential; myrAKT, myristoylated AKT; NMNAT, nicotinamide mononucleotide adenylyltransferase; PI3K, phosphatidylinositol-4,5-bisphosphate 3-kinase; PS, phosphatidylserine; SCG10, superior cervical ganglion 10; TMRM, tetramethylrhodamine methyl ester; UPS, ubiquitin proteasome system; WT, wild type; ZNRF1, zinc and ring finger 1.

The Rockefeller University Press $30.00
J. Cell Biol. Vol. 216 No. 2 477–493
https://doi.org/10.1083/jcb.201606020

Results

MCL1 is a substrate for GSK3B during Wallerian degeneration

The mechanism underlying axonal degeneration is important for understanding the pathogenesis of several neurodegenerative conditions as well as their prevention and treatment. In an attempt to define the molecular mechanism responsible for axonal degeneration, we screened a murine brain cDNA library to identify genes preventing axonal degeneration using an in vitro Wallerian degeneration model (Wakatsuki et al., 2011) and noted that the overexpression of the BCL2 family protein MCL1 delayed axonal degeneration (Fig. 1, A and B). MCL1 is known to be phosphorylated at the 140th serine (S140) by GSK3B (Maurer et al., 2006). Because GSK3B promotes axonal degeneration (Wakatsuki et al., 2011), we hypothesized that MCL1 serves as a GSK3B substrate during the process of Wallerian degeneration. To examine this possibility, we set up an in vitro experiment using the Twiss filter system (Schoenmann et al., 2010), which allows efficient purification of axonal material for biochemical analyses. Using this system, we examined changes in the phosphorylation levels of MCL1 in degenerating axons. We found that increased phosphorylation levels at S140 of MCL1 (MCL1 pS140) in transected axons are clearly inhibited by the application of the GSK3B inhibitor, 4-benzyl-2-methyl-1,2,4-thiadiazolidine-3,5-dione (TDZD), which protects axons from degeneration after transection (Wakatsuki et al., 2011; Fig. 1 C). To confirm that MCL1 pS140 is controlled by GSK3B activity, we examined MCL1 phosphorylation in degenerating axons overexpressing either wild-type (WT) GSK3B or its mutants together with WT MCL1 or MCL1 S140A, which is resistant to GSK3B-dependent phosphorylation (Fig. S1 A). We found that the overexpression of GSK3B K85M, a kinase-dead form of GSK3B, inhibits MCL1 phosphorylation. In contrast, the overexpression of either WT GSK3B or a constitutively active form of GSK3B (GSK3B S9A) up-regulated MCL1 phosphorylation. We also noted that the phosphorylation levels of MCL1 S140A are not affected by the expression of GSK3B S9A. Collectively, these results indicate that MCL1 is a substrate for GSK3B in axons during Wallerian degeneration.

To investigate whether MCL1 pS140 is involved in the progression of Wallerian degeneration, we performed in vitro Wallerian degeneration experiments using dorsal root ganglia (DRG) explant neurons overexpressing MCL1 S140A (Fig. 1, A and B). We found that the expression of this mutant protects axons from degeneration, although more modestly than that of GSK3B K85M. We designed an optic nerve Wallerian degeneration model to confirm the axonal protective effects of the prevention of MCL1 phosphorylation in vivo (Wakatsuki et al., 2011; Fig. 2). By quantifying the remaining axons using immunohistochemistry of βIII-tubulin and an immunoblot analysis of neurofilament M, we found that the overexpression of GSK3B K85M and MCL1 S140A protects axons from degeneration. These results suggest that the inhibition of the GSK3B–MCL1 pathway results in axonal protection against degeneration.

Previous studies reported robust axonal protection through the inhibition of sterile-α and TIR motif–containing protein 1 (SARM1)–elicited signaling (Osterloh et al., 2012). To compare the axonal protective capability of the down-regulation of *sarm1* and inhibition of GSK3B-MCL1 signaling directly, we performed in vitro Wallerian degeneration experiments with the down-regulation of *sarm1* and inhibition of GSK3B-MCL1 signaling side by side. We found that down-regulated expression of *sarm1* protects axons for up to 72 h after transection, whereas inhibition of the GSK3B–MCL1 pathway protects axons for up to 48 h (Fig. 1, A and B). These results suggest that axonal protection afforded through inhibition of the GSK3B–MCL1 pathway is weaker than that by the loss of SARM1.

FBXW7 leads to MCL1 degradation through the UPS during Wallerian degeneration

Previous studies have shown in different cellular contexts that the phosphorylation of MCL1 leads to its release from mitochondria and its degradation via the UPS (Maurer et al., 2006; Germain et al., 2011; Inuzuka et al., 2011). To investigate whether phosphorylation-dependent MCL1 degradation is also observed in axons during Wallerian degeneration, we assessed changes in MCL1 expression levels in the mitochondrial fraction purified from transected axons in culture (Fig. 3 A). We found that mitochondrial MCL1 levels in axons decrease 3 h after transection and that the application of TDZD prevents this reduction. We also noted that the overexpressed MCL1 S140A, but not WT MCL1, is maintained in the mitochondrial fraction of degenerating axons (Fig. 3 B). These results suggest that GSK3B activity reduces the expression levels of mitochondrial MCL1. To investigate whether the degradation of MCL1 is dependent on UPS activity, we assessed MCL1 expression levels in the presence of the proteasomal inhibitor MG132 or lactacystin. We found that reductions in MCL1 expression levels are prevented in the presence of MG132 or lactacystin and that MCL1 is ubiquitinated after transection, which is prevented by the application of TDZD (Fig. 3, C and D; and Fig. S1 B). To confirm these results, we expressed WT MCL1 and its mutants in cultured DRG neurons and examined changes in MCL1 expression levels in transected axons in the presence of MG132 (Fig. 3, E and F). We found that WT MCL1 and MCL1 bearing a S140D mutation (MCL1 S140D) that mimics MCL1 pS140, but not MCL1 S140A, are similarly ubiquitinated. These results indicate that the UPS controls the expression levels of MCL1 in a GSK3B-mediated phosphorylation–dependent manner.

Previous studies identified MCL1 ubiquitin ligase (MULE) and FBXW7 proteins as E3 ubiquitin ligases that target MCL1 for UPS-dependent degradation (Zhong et al., 2005; Inuzuka et al., 2011; Wertz et al., 2011). To elucidate the regulatory mechanism responsible for MCL1 stability, we examined the role of these proteins in the degradation of MCL1 in degenerating axons (Fig. 4, A and B; and Fig. S1, C and D). We found that the RNAi-mediated down-regulation of *fbxw7*, but not *mule*, expression delays axonal degeneration. We detected increased expression levels and decreased polyubiquitinated levels of MCL1 in transected axons from DRG explants expressing shRNA for *fbxw7* (Fig. 4, C–E; and Fig. S1 E), implying a role for FBXW7 in the regulation of MCL1 stability. We also investigated whether the expression levels of mitochondrial MCL1 are affected by the expression of shRNA for *fbxw7* (Fig. 4 F). We found that mitochondrial MCL1, maintaining its expression level, is significantly phosphorylated at S140. Importantly, the application of TDZD to *fbxw7* shRNA-expressing axons decreased the phosphorylation levels of mitochondrial MCL1 without affecting its expression levels. Collectively, these results suggest that FBXW7 recognizes MCL1 when it is phosphorylated at S140 and leads to its degradation via UPS. We performed coimmunoprecipitation experiments using murine neuroblastoma Neuro-2a cells expressing

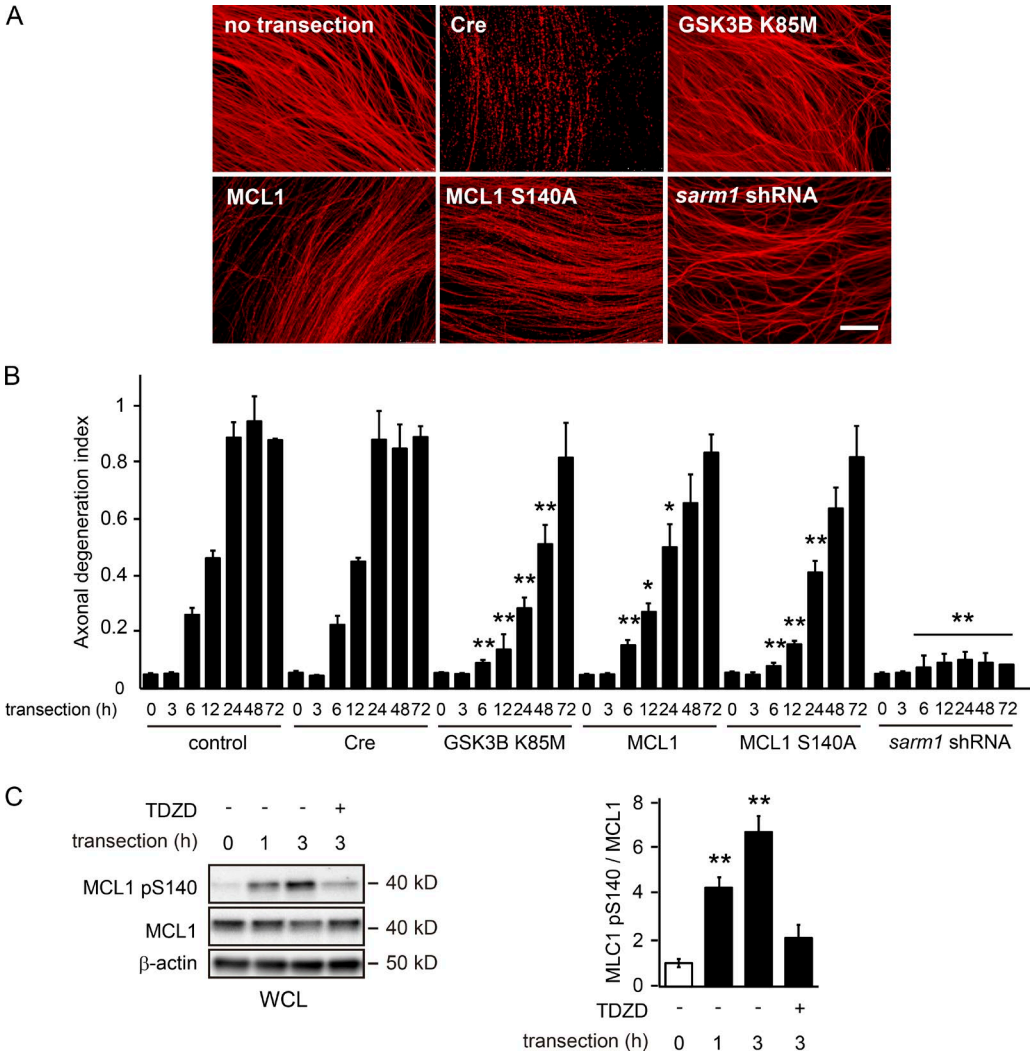

Figure 1. **MCL1 phosphorylation at S140 is involved in the progression of Wallerian degeneration.** (A and B) Axonal protective effects induced by the expression of the indicated genes were assessed by in vitro Wallerian degeneration experiments using axons from cultured DRG explant neurons. Representative photomicrographs of immunostaining against β-tubulin of degenerating axons 24 h after transection are shown in A. Bar, 25 µm. The axonal degeneration index value calculated for each condition at the indicated time point is shown in B (mean ± SEM, *n* = 5). (C) MCL1 is phosphorylated at S140 during Wallerian degeneration. Lysates were prepared from axons at the indicated time points after transection. Representative immunoblots and quantified expression levels for MCL1 pS140 normalized to the MCL1 level relative to the control (open bar; mean ± SEM, *n* = 5) are shown. Significant differences from the control (*, P < 0.05; **, P < 0.01) were determined by one-way analysis of variance with Tukey's post-hoc test. WCL, whole cell lysate.

FBXW7, together with WT MCL1 or its mutant, to demonstrate the direct interaction between FBXW7 and MCL1 (Fig. 4 G). We found that FBXW7 associates more strongly with MCL1 S140D than with WT MCL1, and weakly with MCL1 S140A, suggesting that FBXW7 is directly associated with phosphorylated MCL1. A previous study reported FBXW7-mediated ubiquitination at five lysine residues in human MCL1 (Inuzuka et al., 2011). In an attempt to elucidate the molecular mechanisms underlying the FBXW7-mediated ubiquitination of MCL1 in more detail, we examined the significance of the three lysine residues conserved in murine MCL1 (K117, K175, and K178). We found that these residues are ubiquitinated by FBXW7 (Fig. S1 F). We also found that the coexpression of GSK3B S9A enhances the FBXW7-dependent ubiquitination of MCL1 at K117, K175, and K178. These results collectively suggest that the GSK3B-mediated phosphorylation of MCL1 in degenerating axons leads to the FBXW7-dependent degradation of MCL1 via UPS.

GSK3B-mediated phosphorylation of MCL1 leads to activation of axonal autophagy

The UPS-dependent degradation of MCL1 in the nervous system has previously been demonstrated under different physiological and pathological conditions; the degradation of MCL1 has been correlated with the induction of autophagy under some of these conditions (Germain et al., 2011; Xingyong et al., 2013). Because autophagy is known to be induced in degenerating axons (Yang et al., 2013; Wong and Holzbaur, 2015), we examined the causal relationship between the degradation of MCL1 in degenerating axons and the induction of axonal autophagy. We performed in vitro Wallerian degeneration experiments using cultured DRG neurons dissected from transgenic mice expressing the autophagy marker, the GFP-tagged version of LC3B (GFP-LC3B Tg mice; Mizushima et al., 2004), to assess the induction of autophagy in axons during degeneration (Fig. 5, A and B; and Fig. S2, A and B). We found that the conversion of GFP-LC3B-I into GFP-LC3B-II and the formation

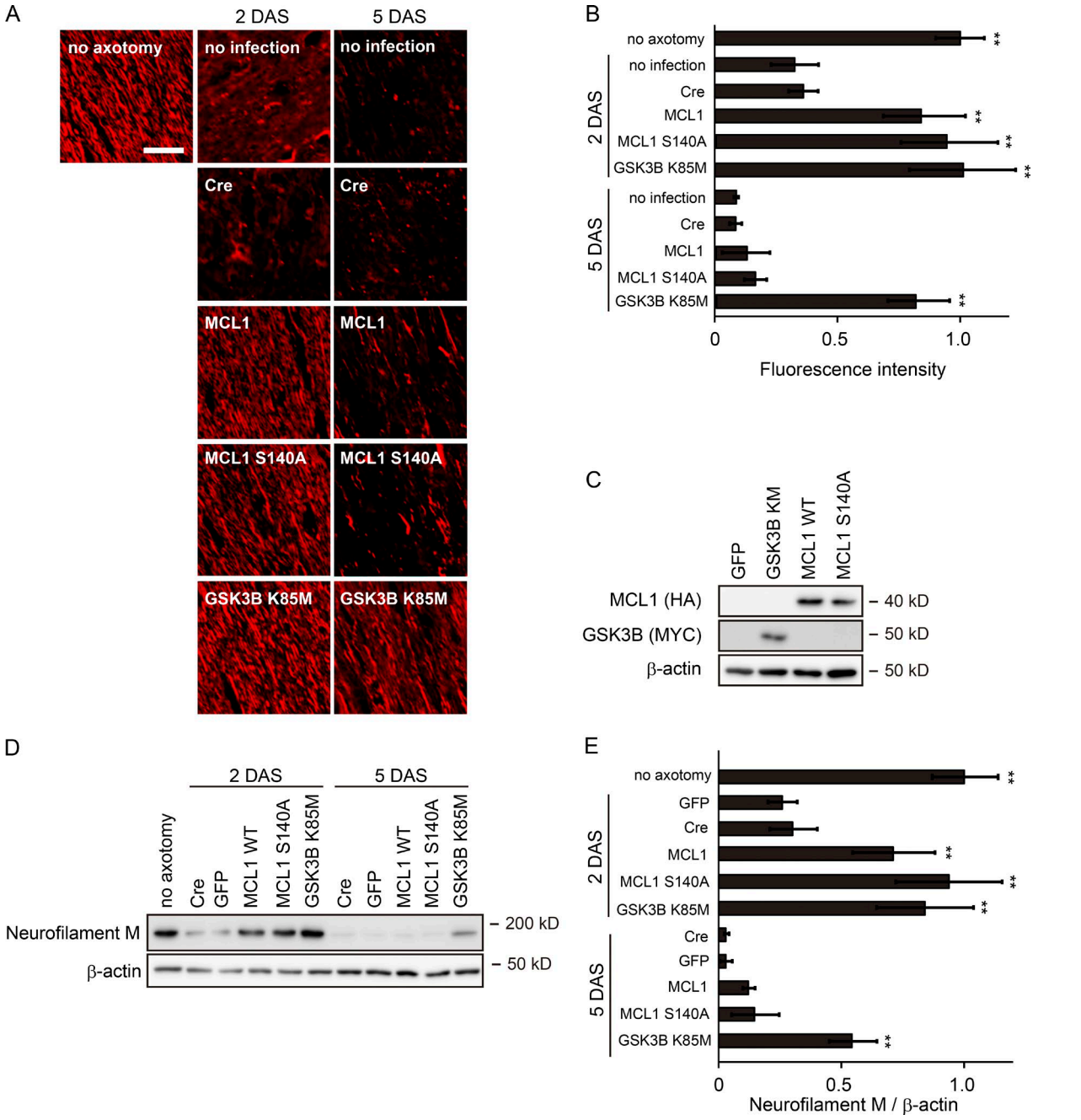

Figure 2. **Inhibition of the GSK3B–MCL1 pathway delays the Wallerian degeneration of optic nerves in vivo.** A unilateral intravitreal injection of adenoviral vector solution for the expression of the indicated molecules in retinal ganglion neurons was performed in adult mice, followed by optic nerve transection 5 d after the injection to induce Wallerian degeneration. Degeneration of the optic nerve (between the eye and optic chiasm) was assessed by the expression of neurofilament M at the indicated time points. DAS, days after surgery. (A) Representative photomicrographs for the immunostaining of neurofilament M on longitudinal optic nerve sections are shown. Bar, 25 µm. (B) Quantified immunofluorescent intensity for each condition relative to the intensity of a "no-axotomy" sample is shown (mean ± SEM, *n* = 5). (C) Representative immunoblots for the expression of the indicated molecules in the optic nerves 5 d after infection is shown. (D) Representative immunoblot for the expression of neurofilament M for each condition is shown. β-Actin served as a loading control. (E) Quantified levels of neurofilament M normalized to β-actin at the indicated time points are shown relative to the no-axotomy condition (mean ± SEM, *n* = 5). We obtained essentially the same results by using βIII-tubulin as a marker for intact axons (not depicted). Significant differences from the control (**, P < 0.01) were determined by one-way analysis of variance with Tukey's post-hoc test.

of GFP-LC3B puncta are decreased in axons expressing myristoylated AKT (myrAKT, a constitutively active form of AKT) or MCL1 S140A, but are increased in GSK3B S9A-expressing axons (Fig. 5, A and B). To determine the nature of the increased LC3-II formation in axons after transection, we used a lysosomal H^+-ATPase inhibitor, bafilomycin A1, to examine autophagic flux. We observed that the LC3-II/LC3-I ratios in axons with no infection and axons expressing GSK3B S9A are increased by bafilomycin A1 treatment (Fig. 5 B). These observations indicate that axonal transection–induced activation of the GSK3B–MCL1 pathway increases autophagy. To demonstrate the relationship between the GSK3B–MCL1 pathway

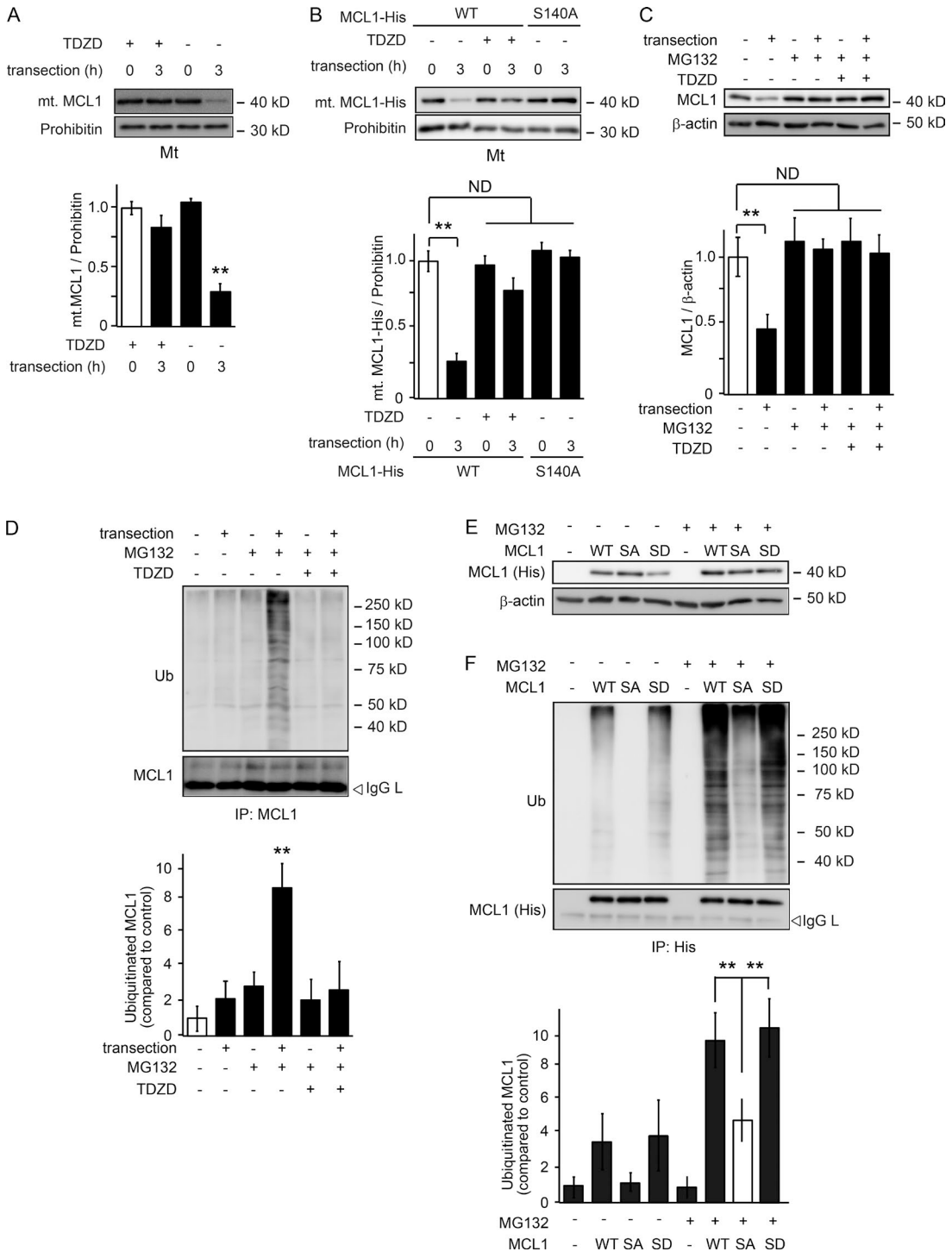

Figure 3. **GSK3B-mediated phosphorylation of MCL1 leads to its degradation via the UPS during Wallerian degeneration.** (A) MCL1 is released from mitochondria after transection. Mitochondrial fractions were prepared from axons at the indicated time points after transection. Representative immunoblots and quantified expression levels for mitochondrial MCL1 normalized to prohibitin relative to the control (mean ± SEM, *n* = 5) are shown. (B) The MCL1 S140A mutant is resistant to release from mitochondria. Lysates were prepared from axons expressing His-tagged WT and the MCL1 S140A mutant at the indicated time points after transection. Representative immunoblots and quantified expression levels for MCL1-His normalized to prohibitin relative to the control (open bar; mean ± SEM, *n* = 5) are shown. (C and D) MCL1 is ubiquitinated after transection. Lysates were prepared from axons 3 h after transection. Representative immunoblots (C) and immunoprecipitation (IP; D) using an anti-MCL1 antibody analyzed by immunoblotting and quantified levels for polyubiquitinated MCL1 normalized to β-actin relative to the control are shown. Note that the ubiquitination of MCL1 was not detected in the presence of TDZD. (E and F) MCL1 pS140 is required for its ubiquitination (Ub). Lysates were prepared from axons overexpressing His-tagged WT and S140A (SA) and S140D (SD) mutant forms of MCL1. Representative immunoblots (E) and immunoprecipitation (F) using an anti-His tag antibody analyzed by immunoblotting and quantified levels for polyubiquitinated MCL1 normalized to β-actin relative to the control are shown. Significant differences from the control (open bar; ** $P < 0.01$) were determined by one-way analysis of variance with Tukey's post-hoc test. IgG L, IgG light chain; Mt, mitochondrial fraction; mt., mitochondrial; ND, not significantly different.

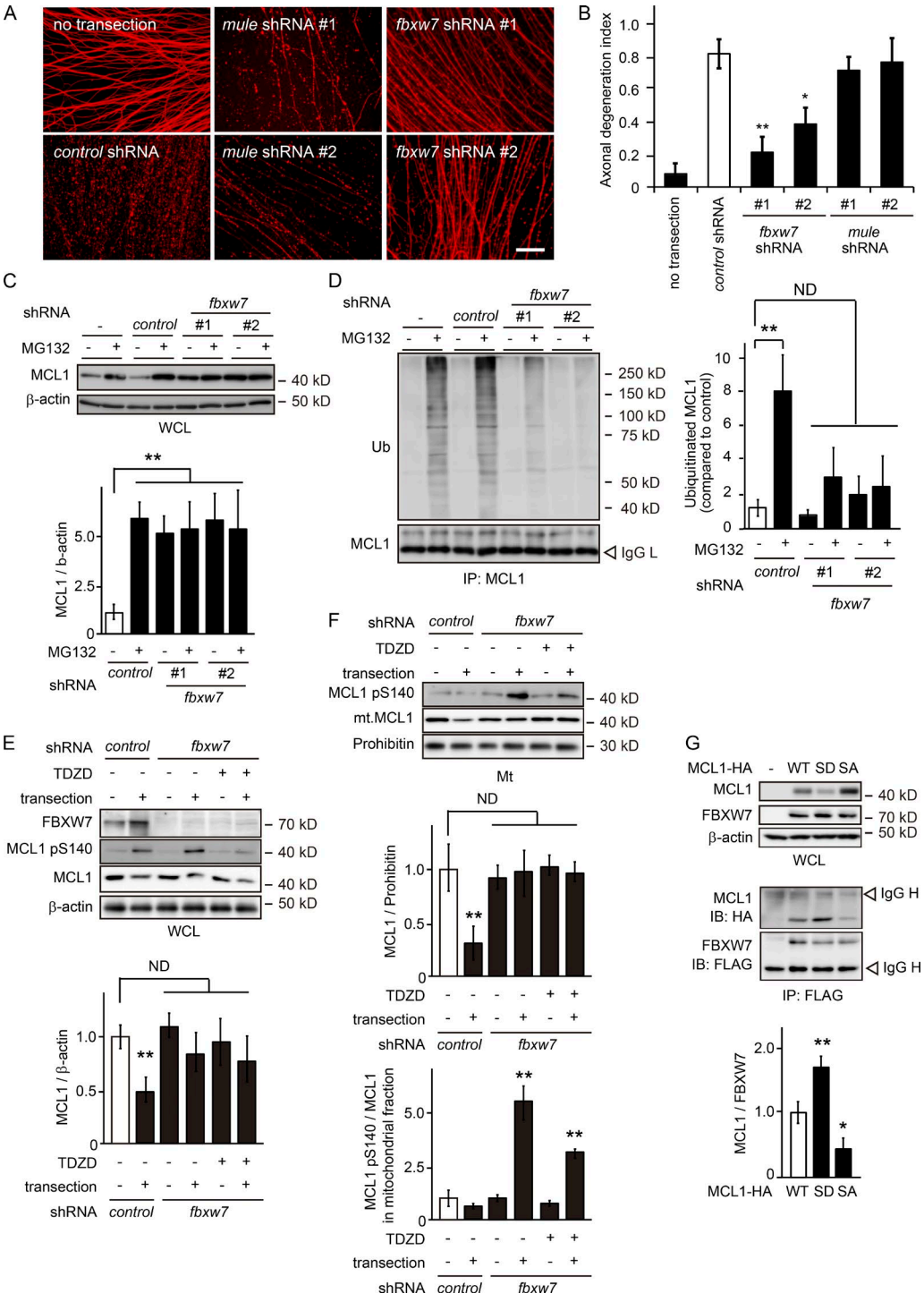

Figure 4. **FBXW7 targets MCL1 pS140 on mitochondria.** (A and B) The down-regulated expression of *fbxw7* inhibits Wallerian degeneration. The degeneration of axons expressing the indicated shRNA was assessed by an in vitro Wallerian degeneration model. Representative photomicrographs for β-tubulin immunostaining of axons are shown in A. Bar, 50 µm. The axonal degeneration index value calculated for each condition 24 h after the induction of degeneration is shown in B. (C and D) The down-regulated expression of *fbxw7* results in an increase in the expression and decrease in the polyubiquitinated (Ub) levels of MCL1 in transected axons. Lysates were prepared from the axons expressing shRNA against *fbxw7*. Representative immunoblots (C) and immunoprecipitation (D) using an anti-MCL1 antibody analyzed by immunoblotting and quantified levels for MCL1 or polyubiquitinated MCL1 normalized to β-actin relative to the control are shown. (E) The down-regulated expression of *fbxw7* stabilizes MCL1. Representative immunoblots and quantified expression levels of MCL1 normalized to β-actin relative to the control (open bar) are shown (mean ± SEM, $n = 3$). (F) The down-regulated expression of *fbxw7* inhibits MCL1 release from mitochondria. Mitochondrial fractions were prepared from axons expressing shRNA against *fbxw7*. Representative immunoblots (top) and quantified expression levels of MCL1 normalized to prohibitin (middle) or MCL1 pS140 normalized to MCL1 (bottom) relative to the control (open bar) in mitochondrial fractions are shown (mean ± SEM, $n = 5$). (G) Demonstration of the direct interaction between FBXW7 and MCL1 in murine neuroblastoma Neuro-2a cells. Representative immunoblots (IB) and immunoprecipitation using an anti-FLAG antibody analyzed by immunoblotting and quantified levels for MCL1-HA normalized to FLAG-FBXW7 relative to the control (open bar) are shown (mean ± SEM, $n = 5$). Significant differences from the control (*, $P < 0.05$; **, $P < 0.01$) were determined by one-way analysis of variance with Tukey's post-hoc test. Mt, mitochondrial; ND, not significantly different; SA, S140A; SD, S140D; WCL, whole cell lysate.

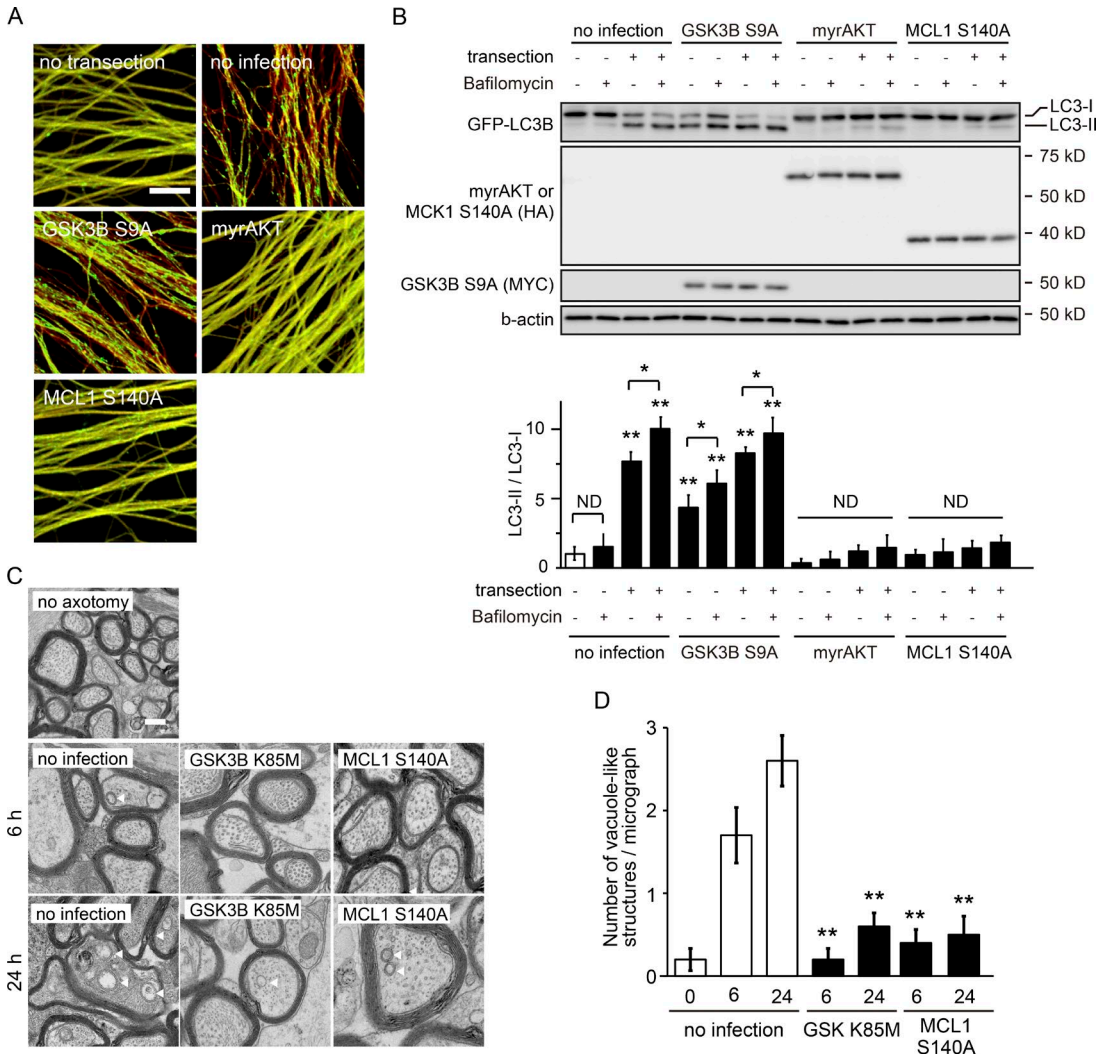

Figure 5. **GSK3B-mediated phosphorylation of MCL1 leads to activation of axonal autophagy.** (A and B) The GSK3B–MCL1 pathway regulates the induction of autophagy in transected axons. Axonal autophagic activity was assessed in degenerating axons in vitro using cultured DRG neurons from GFP-LC3B Tg mice. Representative photomicrographs for GFP and immunostaining against β-tubulin (red) of degenerating axons expressing the indicated molecules are shown in A. Bar, 10 µm. Lysates were prepared from cultured GFP-LC3B Tg DRG axons before and 3 h after transection. Representative immunoblots and quantified levels for GFP-LC3II normalized to GFP-LC3B-I relative to the control (open bar) are shown (mean ± SEM, $n = 5$) in B. (C and D) Inhibition of the GSK3B–MCL1 pathway prevents autophagosome-like vacuole formation in the degenerating optic nerve axons in vivo. A unilateral intravitreal injection of adenoviral vector solution for the expression of the indicated molecules in retinal ganglion neurons was performed in adult mice, followed by optic nerve transection 5 d after the injection to induce Wallerian degeneration. Autophagosome formation in optic nerve axons (between the eye and optic chiasm) was assessed by electron microscopy at the indicated time points. Representative photomicrographs for an electron microscopic analysis of transverse optic nerve sections are shown in C. Arrowheads indicate autophagosome-like vacuoles in C. Bar, 1 µm. The number of autophagosomes to optic nerve axons under each condition is shown in (D; mean ± SEM, $n = 3$). Significant differences from the control (*, $P < 0.05$; **, $P < 0.01$) were determined by one-way analysis of variance with Tukey's post-hoc test. ND, not significantly different.

and the induction of axonal autophagy in vivo, we performed ultrastructural analyses using an optic nerve Wallerian degeneration model (Wakatsuki et al., 2011; Fig. 5, C and D). Autophagosome-like vacuoles were identified as vesicular structures with a delimiting double membrane with a typical diameter of 0.5–1 µm (Komatsu et al., 2007; Mizushima et al., 2010) in the optic nerve axons 24 h after transection; however, these structures were not observed in axons infected with an adenovirus expressing GSK3B K85M and MCL1 S140A. Although we have yet to determine the exact nature of these structures, these results suggest that the GSK3B–MCL1 pathway leads to the formation of autophagosome-like vacuoles in axons during Wallerian degeneration in vivo. We also found that overexpression of the BCL2 family proteins BCL2 and BCLW did not rescue the effects of the down-regulated expression of *mcl1* on axonal autophagy (Fig. 6). Collectively, these results suggest that axonal autophagy is regulated by MCL1, which cannot be compensated for by BCL2 or BCLW.

To directly correlate the FBXW7-dependent degradation of MCL1 with axonal autophagy, we examined the effects of *fbxw7* down-regulation on axonal autophagy using in vitro Wallerian degeneration experiments (Fig. 7). We found that the conversion of GFP-LC3B-I to GFP-LC3B-II, the formation of GFP-LC3B puncta, and the degradation of an autophagic substrate p62 are decreased in *fbxw7*–down-regulated axons (Fig. 7, C and D). The induction of autophagy is mediated through canonical and noncanonical pathways (Nishida et al., 2009; Mizushima et al., 2010). The deficiencies in key

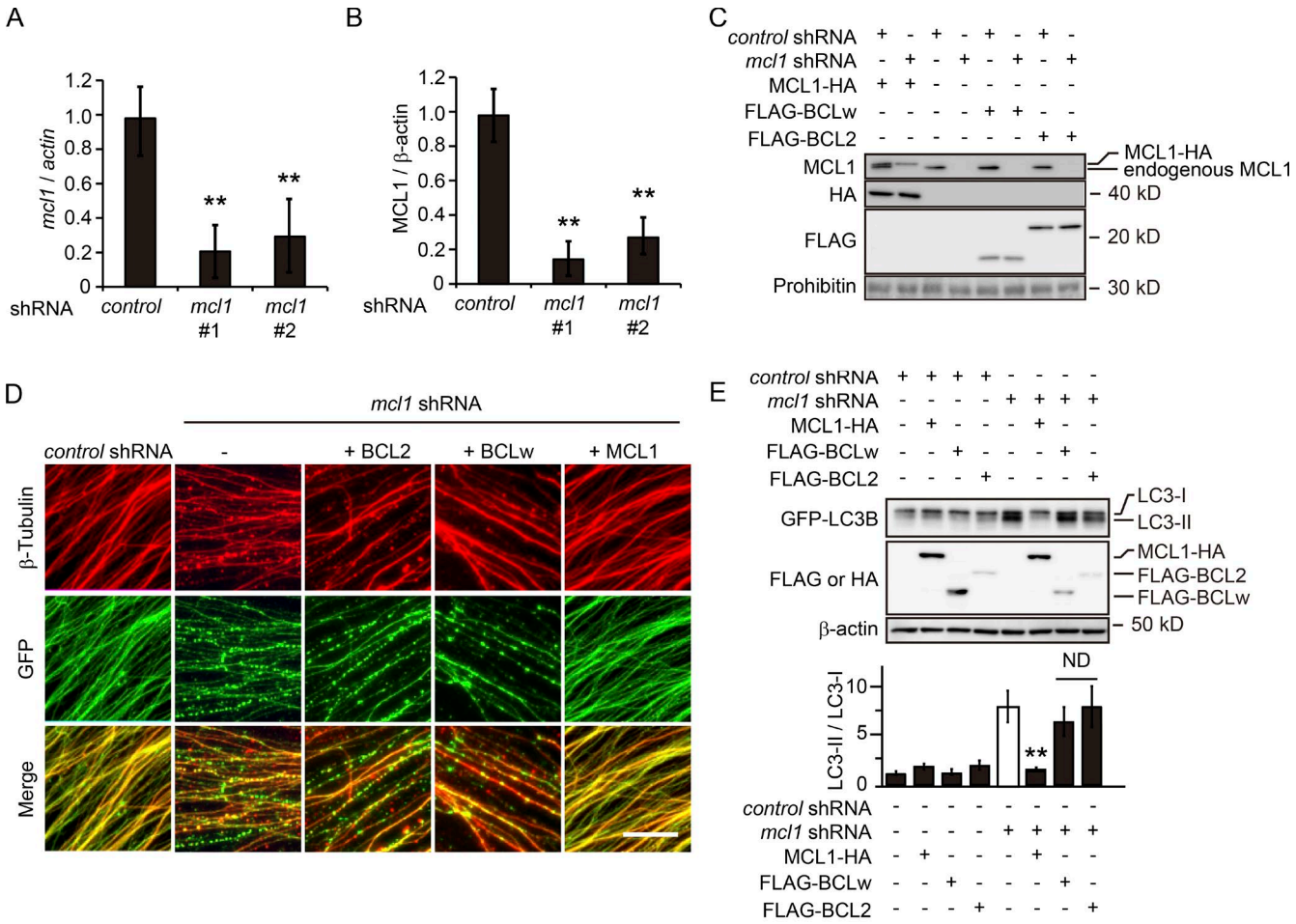

Figure 6. **The GSK3B–MCL1 pathway is involved in injury-induced axonal autophagy.** (A–C) The down-regulated expression of *mcl1* by specific shRNA in cultured DRG neurons by the two independent shRNAs used in this study was confirmed by quantitative RT-PCR (A) and immunoblot analysis (B and C). Expression levels of *mcl1* normalized to β-actin relative to those of the nontarget control shRNA-expressing condition are shown in A (mean ± SEM, $n = 5$). Lysates prepared from the axons expressing the indicated molecules were examined by immunoblot analysis using the indicated antibodies. Representative images of immunoblots (C) and quantified expression level of MCL1 normalized to β-actin relative to that of the nontarget control shRNA-expressing condition (B) are shown. (D and E) Axonal autophagic activity during Wallerian degeneration in vitro was assessed using cultured GFP-LC3B Tg DRG neurons. Representative photomicrographs for GFP and immunostaining against β-tubulin (red) of degenerating axons expressing the indicated molecules are shown in D. Bar, 10 µm. Lysates prepared from the axons of cultured GFP-LC3B Tg DRG neurons were subjected to immunoblot analysis using the indicated antibodies. Representative immunoblots and quantified levels for GFP-LC3B-II normalized to GFP-LC3B-I relative to the control (open bar) are shown in E (mean ± SEM, $n = 5$). Note that the reduced expression of MCL1 in neurons expressing shRNA for MCL1 was rescued by the expression of shRNA-resistant MCL1. Significant differences from the control (**, $P < 0.01$) were determined by one-way analysis of variance with Tukey's post-hoc test. ND, not significantly different.

Atg genes, such as *atg5* (Mizushima et al., 2001; Kuma et al., 2004) and *atg7* (Komatsu et al., 2005), are known to impair canonical autophagy. To analyze whether FBXW7-dependent degradation of MCL1 leads to canonical autophagy in axons, we examined the effects of down-regulating the expression of *atg5* or *atg7* on axonal autophagy (Fig. 7, A–D). We found that down-regulation of *atg5* or *atg7* suppresses axonal degeneration to an extent similar to that by the down-regulation of *fbxw7* expression (Fig. 7, E–H). We also found that treatment with a phosphatidylinositol-4,5-bisphosphate 3-kinase (PI3K) inhibitor, 3-methyladenine, results in axonal protection from degeneration (Fig. S2, C and D). These results suggest that canonical autophagy mediated by FBXW7-dependent degradation of MCL1 promotes axonal degeneration. To examine whether autophagy induction is sufficient to promote axonal degeneration, we tried to induce autophagy in intact axons in culture. Because methods to induce autophagy in neurons have not previously been established (Yang et al., 2013; Maday and Holzbaur, 2016), we chose to down-regulate *mcl1* by RNAi or overexpress MCL1 S140D in cultured DRG neurons. We found that *mcl1* down-regulation or MCL1 S140D expression induces axonal autophagy and subsequent degeneration (Fig. S2, E–H). Interestingly, autophagy-induced axonal degeneration required a longer period of time to complete than axotomy-induced degeneration, and *mcl1* down-regulation–induced axonal degeneration was prevented by the expression of shRNA-resistant MCL1 (Fig. S2, G and H). Importantly, we also found that the axonal degeneration caused by MCL1 S140D expression was suppressed by inhibition of autophagy by down-regulation of *atg5* or *atg7* (Fig. S2, E and F). Because the suppression of MCL1 S140D expression–induced axonal degeneration by autophagy inhibition appears to be incomplete, autophagy in-

duction may not be the only signaling pathway downstream of MCL1 phosphorylation and degradation. These results suggest that FBXW7-dependent degradation of MCL1 in response to axonal injury induces canonical autophagy in axons to promote axonal degeneration.

Dissociation of MCL1 with BECLIN1 in axons leads to the induction of autophagy

Previous studies have shown that MCL1 inhibits autophagy through an interaction with BECLIN1, a key regulator of autophagy, and dissociation of BECLIN1 from MCL1 induces autophagy (He and Levine, 2010; Germain et al., 2011; Kang et al., 2011; Tai et al., 2013). To examine changes in the molecular interaction between MCL1 and BECLIN1 in axons during degeneration, we performed coimmunoprecipitation experiments on MCL1 and BECLIN1 from axonal preparations (Fig. 8 A). The interaction between MCL1 and BECLIN1 became weaker after transection. This reduction was prevented by the expression of myrAKT but was accelerated by that of GSK3B S9A. We also found that levels of MCL1 pS140 were increased by the expression of GSK3B S9A, but not by that of myrAKT. To confirm these results, we examined changes in the interactions between transgene-derived MCL1 molecules and endogenous BECLIN1 in transected axons (Fig. 8 B). Although BECLIN1 interacted with MCL1 and MCL1 S140A molecules in a similar manner before transection, only the interaction between BEC LIN1 and MCL1 S140A, and not that with WT MCL1, was maintained 3 h after transection. We also found that the BCL2 homology domain 3 mimetic peptide, ABT-737 (which induces the dissociation of the BCL2 family proteins BCL2 and BCLW, but not MCL1, from BECLIN1 [van Delft et al., 2006]), did not induce axonal autophagy (unpublished data), further supporting the model that the dissociation of MCL1 with BECLIN1 in axons leads to the induction of autophagy. To examine whether MCL1 phosphorylation at S140 is required for dissociation of MCL1 from BECLIN1, we examined MCL1–BECLIN1 interaction in injured axons with *fbxw7* down-regulation (Fig. 8 C). We found that interaction between BECLIN1 and MCL1 pS140 in the *fbxw7*–down-regulated axons was detected 3 h after transection. These results suggest that MCL1 is phosphorylated at S140 while it is associated with BECLIN1. Collectively, our data suggest that the phosphorylation of MCL1 at S140 is required for its subsequent FBXW7-dependent UPS degradation, but the phosphorylation is not enough for dissociation from BECLIN1. We speculate that phosphorylated MCL1 is dissociated from BECLIN1 after MCL1 is ubiquitinated in a FBXW7-dependent manner.

BECLIN1 is known to interact with the class III PI3K VPS34, and targets it to different steps of the autophagic process, such as autophagosome biogenesis and maturation, by forming distinct protein complexes (He and Levine, 2010; Tai et al., 2013). To examine the composition of MCL1- and BEC LIN1-containing complexes during the progression of axonal autophagy, we performed coimmunoprecipitation experiments using MCL1 and BECLIN1 endogenously expressed in axons (Fig. S3, A–C). We found that MCL1 coprecipitates with BEC LIN1 and VPS34 from axons before, but not after, transection. Similarly, BECLIN1 coprecipitated with MCL1 and VPS34 from axons before transection, but not with MCL1 after transection. These results demonstrate that MCL1 interacts with the BECLIN1-containing complex in axons before, but not after, transection, suggesting that MCL1 inhibits autophagy through the interaction with BECLIN1 in healthy axons, and their dissociation upon the induction of Wallerian degeneration initiates axonal autophagy.

Previous studies have shown that FBXW7 plays a regulatory role in mitophagy (Ekholm-Reed et al., 2013; Ivatt et al., 2014). To analyze whether FBXW7-dependent mitophagy is implicated in injury-induced axonal autophagy, we examined colocalization of autophagy marker LC3 with mitochondria in Parkin-overexpressing DRG neurons in culture after injury. We found that neither GFP-LC3B (Fig. S3 D) nor Parkin (unpublished data) colocalizes with mitochondria after transection, even in the *fbxw7* down-regulated axons. These observations exclude the possibility that inhibition of *fbxw7* expression in axons alters mitochondrial function to induce Parkin-dependent mitophagy in axons, at least in our current experimental conditions.

Inhibition of axonal autophagy disrupts local ATP production and subsequent PS exposure

Wallerian degeneration is an active mechanism that requires energy-consuming enzymatic reactions (Wang et al., 2012; Conforti et al., 2014; Gerdts et al., 2016). However, axonal transport is often disrupted in degenerating axons, resulting in a reduction in axonal energy supply. Because the products of autophagic degradation, including amino acids, contribute to the tricarboxylic acid cycle to generate ATP (Lum et al., 2005), we hypothesized that the induction of axonal autophagy may contribute to local ATP production to promote Wallerian degeneration. To examine this possibility, we performed a luciferase-based ATP measurement in axons during degeneration. Although axonal ATP levels showed a continuous reduction after transection, as previously reported (Wang et al., 2005; Yang et al., 2015), we found that axonal ATP levels were maintained within the initial 3 h after transection (Fig. 9, A and B). This phenomenon may be caused by the induction of axonal autophagy after transection, because the transient increase in axonal ATP levels was completely suppressed by a manipulation that inhibits autophagy (Fig. 9 B). To confirm that this transient ATP increase is independent of mitochondrial ATP production, we examined axonal ATP levels in injured axons treated with a mitochondrial H^+-ATP synthase inhibitor, oligomycin (Fig. S4 A). We found that the transient ATP increase is present in the oligomycin-treated injured axons as well. These results are consistent with our hypothesis that autophagy induced in degenerating axons may play a role in energy production required for the progression of Wallerian degeneration.

Dying cellular structures, including axonal debris, are rapidly cleared from the body by phagocytes. In this process, phagocytes recognize eat-me signals such as PS on dying cells (Ravichandran, 2011). Autophagy has been implicated in PS exposure on apoptotic cells (Qu et al., 2007; Mellén et al., 2008). Using in vitro Wallerian degeneration experiments, we found a significant increase in PS exposure on axons 3 h after transection (Fig. 9 C). We also found that the reduction in autophagic activity using shRNAs against *atg5*, *atg7*, and *fbxw7* prevents PS exposure (Fig. 9, D and E), implicating autophagy in PS exposure. The injury-induced PS exposure is observed in oligomycin-treated conditions as well, suggesting that PS exposure is independent of mitochondrial ATP production remaining in the axons (Fig. S4 B). We also found that mitochondrial ATP production (2.22 ± 0.17 pmol/µg of protein in axons expressing shRNA for *fbxw7* vs. 2.31 ± 0.12 pmol/µg of protein in axons

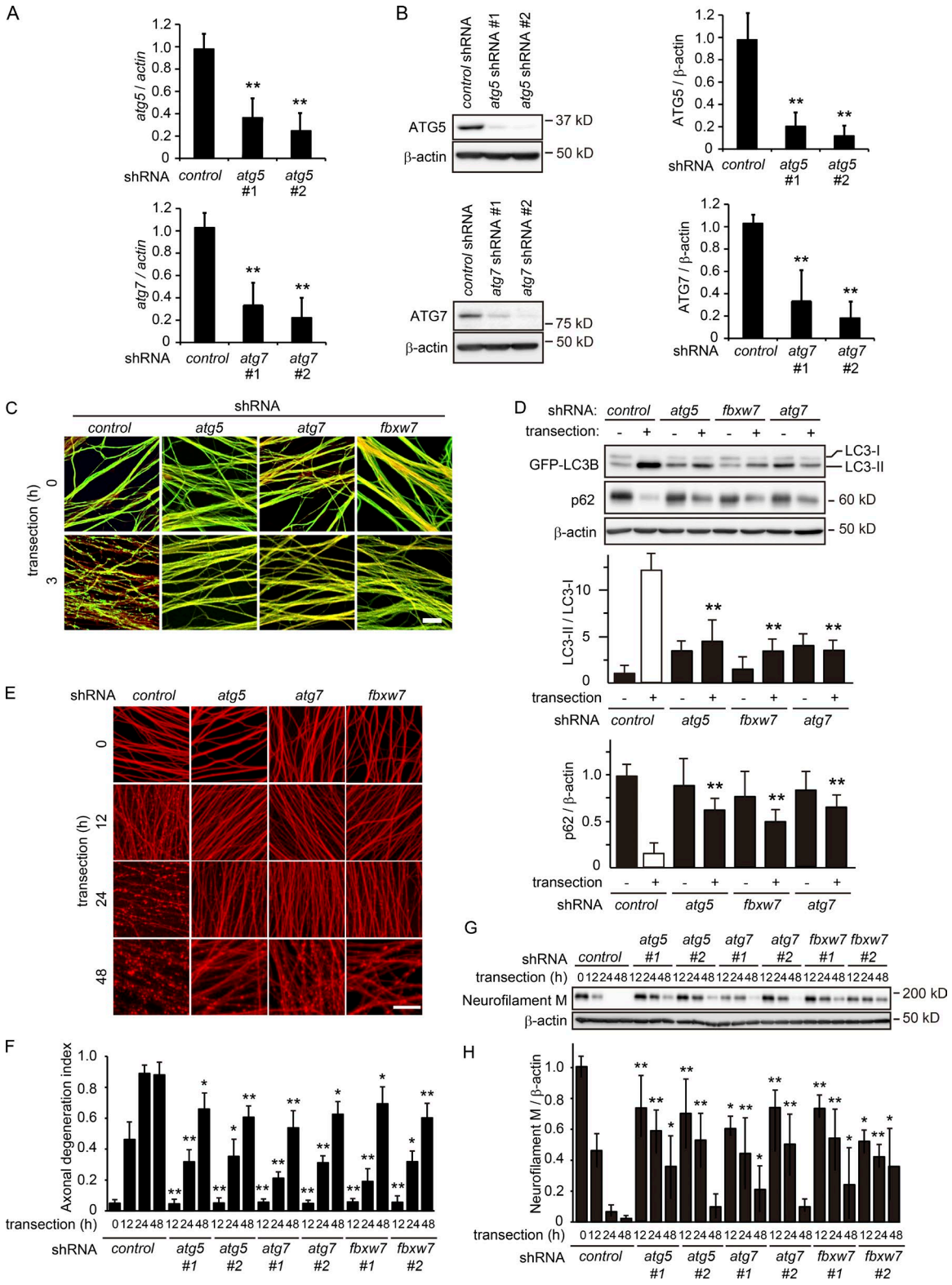

Figure 7. **Down-regulated expression of *fbxw7* prevents autophagy and axonal degeneration.** (A and B) The down-regulated expression of *atg5* and *atg7* by the two independent shRNAs used in this study was confirmed by quantitative RT-PCR (A) and immunoblot analysis (B). The expression level of each molecule normalized to β-actin is shown relative to that of the no-infection condition in A (mean ± SEM, $n = 5$). Representative immunoblots for the analysis of lysates prepared from axons expressing shRNA against *atg5* and *atg7* are shown in B. β-Actin serves as a loading control. The expression level of each molecule normalized to β-actin relative to that of the nontarget control shRNA-expressing condition is also shown (mean ± SEM, $n = 3$). (C and D) Axonal autophagy activity with the shRNA-mediated down-regulation of *fbxw7* expression was assessed using an in vitro Wallerian degeneration model. Representative photomicrographs for GFP and immunostaining of β-tubulin in degenerating axons of cultured GFP-LC3B Tg DRG neurons are shown in C. Bar, 10 µm. Lysates prepared from axons were subjected to immunoblot analysis using the indicated antibodies. Representative immunoblots (top) and quantified expression levels for GFP-LC3B-II (middle) normalized to GFP-LC3B-I or p62 (bottom) normalized to β-actin relative to the control are shown in D (mean ± SEM,

expressing shRNA for nontarget control, mean ± SEM; P = 0.339, $n = 5$) and levels of mitochondrial membrane potential (MMP; Fig. S4 C) are not affected in *fbxw7*–down-regulated axons, suggesting that FBXW7 does not affect mitochondrial ATP production in this experimental context. We observed an increase in ATP levels, but not PS exposure, in *sarm1*–down-regulated axons after transection (Fig. 9, B, D, and E). A previous study demonstrated that the activation of SARM1 resulted in extracellular Ca^{2+} influx into axons after transection (Yang et al., 2015). Because PS exposure is an ATP- and Ca^{2+}-dependent process (Daleke and Lyles, 2000; Elliott et al., 2005; Suzuki et al., 2013), these results suggest that axonal autophagy and SARM1 pathways cooperate to induce PS exposure on axons after the initiation of Wallerian degeneration.

Inhibition of axonal autophagy in optic nerves deteriorates the recruitment of phagocytes to axonal debris in vivo

Inhibition of the GSK3B–MCL1 pathway disrupts local ATP production in degenerating axons and subsequent PS exposure, suggesting that the recruitment of phagocytes to axonal debris is affected by a manipulation that inhibits this pathway in vivo. We investigated this in an optic nerve Wallerian degeneration model coimmunostained with βIII-tubulin and the macrophage marker F4/80 (Fig. 10). By quantifying the recruitment of phagocytes to axonal debris, we found that the clearance of degenerate axons 2 d after axotomy is decreased by the expression of GSK3B K85M and MCL1 S140A (i.e., inhibition of the GSK3B–MCL1 pathway). We obtained similar results by the down-regulation of *atg5*, *atg7*, or *fbxw7* expression in optic nerve axons. These results suggest that the inhibition of axonal autophagy affects the recruitment of phagocytes to axonal debris in vivo.

Discussion

Here, we showed that GSK3B–MCL1 signaling to regulate autophagy plays a role in successful completion of Wallerian degeneration (Fig. S5). The mechanism downstream of GSK3B-dependent MCL1 phosphorylation at S140 is rather complex. MCL1 phosphorylation seems to occur on mitochondria, whereas MCL1 is associated with BECLIN1. BECLIN1 is presumably dissociated from MCL1 upon FBXW7-dependent ubiquitination, and activates autophagy in axons. The injury-induced axonal autophagy seems unique in that Parkin-dependent mitophagy is not involved. Although FBXW7 was previously reported to affect mitochondrial functions and regulate autophagy in certain situations, we observed that the injury-induced axonal autophagy is independent of mitochondrial dysfunction–elicited mechanisms. Instead, we demonstrated novel significance of axonal autophagy during Wallerian degeneration. Axonal autophagy contributes to the production of ATP, which is required to promote degeneration. We showed that axonal autophagy is critical for PS exposure on degenerating axons to recruit phagocytes to the injury site.

Our current results suggest that autophagy promotes Wallerian degeneration. We observed that it takes much longer for autophagy-elicited axonal degeneration to execute than for injury-induced degeneration; although it takes hours to a few days for injury-induced axonal degeneration to complete in culture, it takes 4–7 d for autophagy-induced degeneration. This difference in the time course may explain the partial axonal protective effect for injury-induced degeneration by inhibiting GSK3B–MCL1 signaling or autophagy. Our hypothesis is that axonal transection activates both autophagy and other mechanisms including cytoskeletal degradation (Wakatsuki et al., 2011), and because mechanisms other than autophagy contribute to degrade axons very fast to complete axonal destruction, autophagy inhibition can show a partial protective effect in a relatively early phase of axonal destruction.

The slow progression of autophagy-induced axonal degeneration may seem contradictory to our own data that autophagy induction signals, including MCL1 phosphorylation, become detectable in axons only 3 h after transection. We speculate that, whereas autophagy degrades proteins and organelles in axons to promote axonal degeneration on the one hand, axonal ATP levels are maintained because of autophagy-dependent ATP production (as we show in Fig. 9), which may contribute to maintain enzymatic activities in axons to prevent them from rapid degeneration, on the other hand. Another possibility to explain the slow progression of autophagy-induced axonal degeneration is that autophagy may promote axonal degeneration by degrading key molecules for axonal survival, including NMNAT2 and SCG10 (Shin et al., 2012; Xiong et al., 2012; Conforti et al., 2014). Previous studies have shown that these short half-life proteins are rapidly lost in axons after transection, which results in rapid axonal degeneration. In the case of autophagy-induced axonal degeneration, the expression of these molecules is likely decreased gradually, because protein synthesis and axonal transport are not immediately lost by activation of autophagy. The molecular mechanism of slow execution of autophagy-induced axonal degeneration and its pathophysiological significance may need to be clarified in future studies for complete understanding of axonal degeneration mechanisms and development of axonal protection therapies against neuronal disorders.

Materials and methods

Animals

All animals were maintained in accordance with the guidelines of the National Center for Neurology and Psychiatry. The technical protocols for animal experiments in this study were approved by a review committee for Animal Resources in the National Center for Neurology and Psychiatry. The GFP-LC3B Tg mouse strain (GFP-LC3 #53;

$n = 5$). (E–H) Down-regulation of expression of key Atg genes prevents axonal autophagy. Axonal degeneration with shRNA-mediated down-regulation of *atg5*, *atg7*, or *fbxw7* expression was assessed by immunocytochemistry for β-tubulin (E and F) and immunoblot for neurofilament M (G and H) using an in vitro Wallerian degeneration model. Nontarget control shRNA-infected neurons served as a negative control. Representative photomicrographs of axons are shown in E. Bar, 20 µm. Axonal degeneration index value calculated for each condition at the indicated time point after transection is shown in F. (G and H) Lysates were prepared from axons at the indicated time points after transection and analyzed by immunoblot. Representative immunoblots using the indicated antibodies and relative expression levels for neurofilament M normalized to β-actin are shown (mean ± SEM, $n = 5$). Significant differences from the control (*, P < 0.05; **, P < 0.01) were determined by one-way analysis of variance with Tukey's post-hoc test.

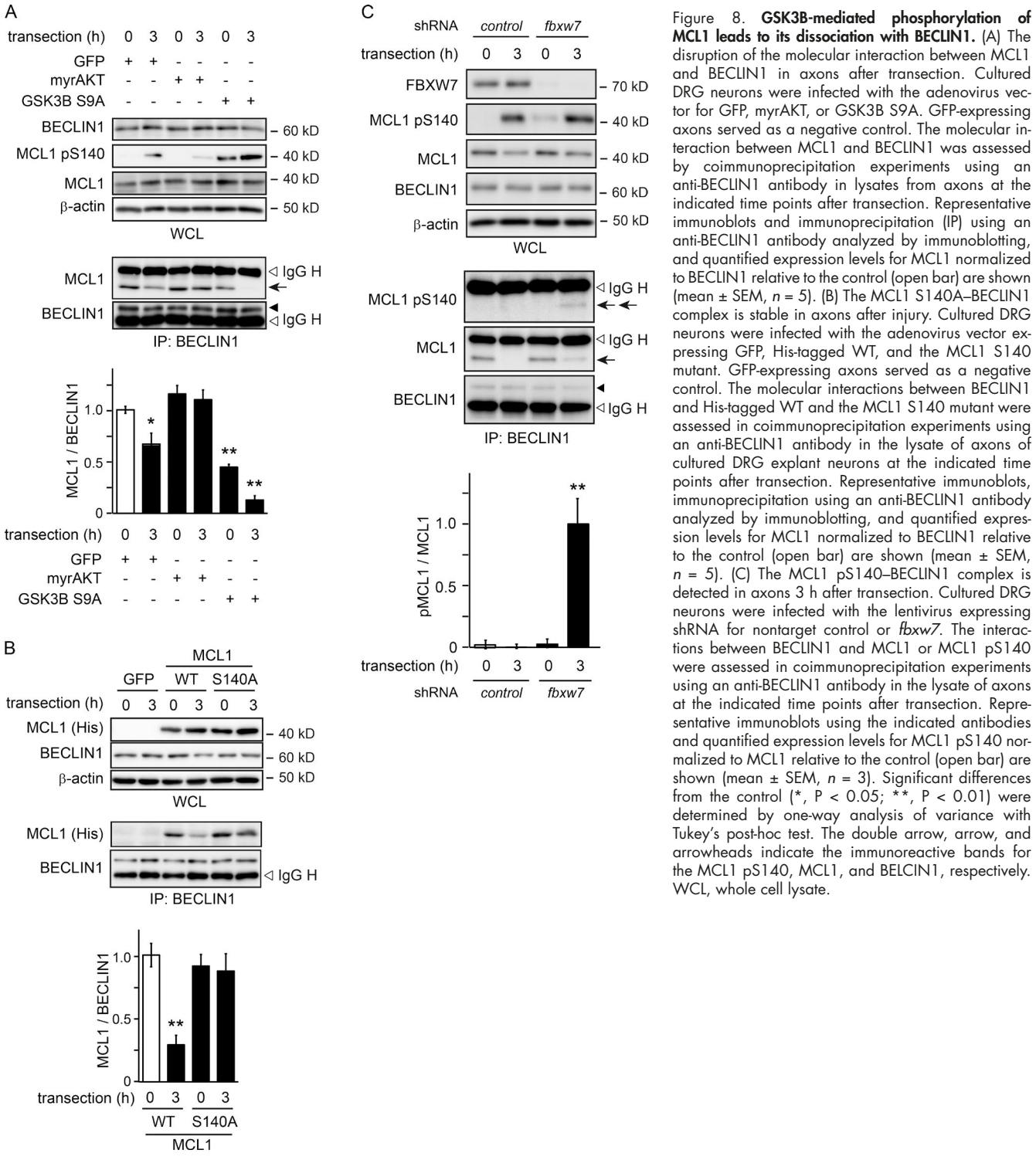

Figure 8. **GSK3B-mediated phosphorylation of MCL1 leads to its dissociation with BECLIN1.** (A) The disruption of the molecular interaction between MCL1 and BECLIN1 in axons after transection. Cultured DRG neurons were infected with the adenovirus vector for GFP, myrAKT, or GSK3B S9A. GFP-expressing axons served as a negative control. The molecular interaction between MCL1 and BECLIN1 was assessed by coimmunoprecipitation experiments using an anti-BECLIN1 antibody in lysates from axons at the indicated time points after transection. Representative immunoblots and immunoprecipitation (IP) using an anti-BECLIN1 antibody analyzed by immunoblotting, and quantified expression levels for MCL1 normalized to BECLIN1 relative to the control (open bar) are shown (mean ± SEM, $n = 5$). (B) The MCL1 S140A–BECLIN1 complex is stable in axons after injury. Cultured DRG neurons were infected with the adenovirus vector expressing GFP, His-tagged WT, and the MCL1 S140 mutant. GFP-expressing axons served as a negative control. The molecular interactions between BECLIN1 and His-tagged WT and the MCL1 S140 mutant were assessed in coimmunoprecipitation experiments using an anti-BECLIN1 antibody in the lysate of axons of cultured DRG explant neurons at the indicated time points after transection. Representative immunoblots, immunoprecipitation using an anti-BECLIN1 antibody analyzed by immunoblotting, and quantified expression levels for MCL1 normalized to BECLIN1 relative to the control (open bar) are shown (mean ± SEM, $n = 5$). (C) The MCL1 pS140–BECLIN1 complex is detected in axons 3 h after transection. Cultured DRG neurons were infected with the lentivirus expressing shRNA for nontarget control or *fbxw7*. The interactions between BECLIN1 and MCL1 or MCL1 pS140 were assessed in coimmunoprecipitation experiments using an anti-BECLIN1 antibody in the lysate of axons at the indicated time points after transection. Representative immunoblots using the indicated antibodies and quantified expression levels for MCL1 pS140 normalized to MCL1 relative to the control (open bar) are shown (mean ± SEM, $n = 3$). Significant differences from the control (*, $P < 0.05$; **, $P < 0.01$) were determined by one-way analysis of variance with Tukey's post-hoc test. The double arrow, arrow, and arrowheads indicate the immunoreactive bands for the MCL1 pS140, MCL1, and BELCIN1, respectively. WCL, whole cell lysate.

Mizushima et al., 2004) was provided by the Institute of Physical and Chemical Research BioResource Center (RBRC00806).

Antibodies

The antibodies used and their sources are as follows: mouse anti–β-actin (622101; BioLegend); rabbit anti–βIII-tubulin (802001; BioLegend); mouse anti-ubiquitin (MMS-258R; Covance; or clone FK2; Enzo Life Sciences); mouse anti–HA-tag (MMS-101R; Covance); mouse anti–β-tubulin (clone E7; DSHB); rabbit anti–neurofilament M (AB1987; EMD Millipore); mouse anti–MYC-tag (clone 9E10; DSHB); mouse anti–FLAG-tag (clone M2; Sigma-Aldrich); rabbit anti-GFP (598; MBL); rabbit anti-FBXW7 (ab109617; Abcam); rabbit anti-HUWE1/MULE (sc-49768; Santa Cruz Biotechnology, Inc.); rabbit anti-BECLIN1 (PD017; MBL); rabbit anti-VPS34 (GTX129528; GeneTex); rabbit anti-BCL2 (50E3; Cell Signaling Technology); rabbit anti-MCL1 (ABIN126984; antibodies-online.com); rabbit anti–phospho-MCL1 (SAB4504259; Sigma-Aldrich); mouse anti-prohibitin (Clone II-14-10; Thermo Fisher Scientific); rabbit anti-p62 (PM045; MBL); rabbit anti-ATG5 (2630; Cell Signaling Technology); and rabbit

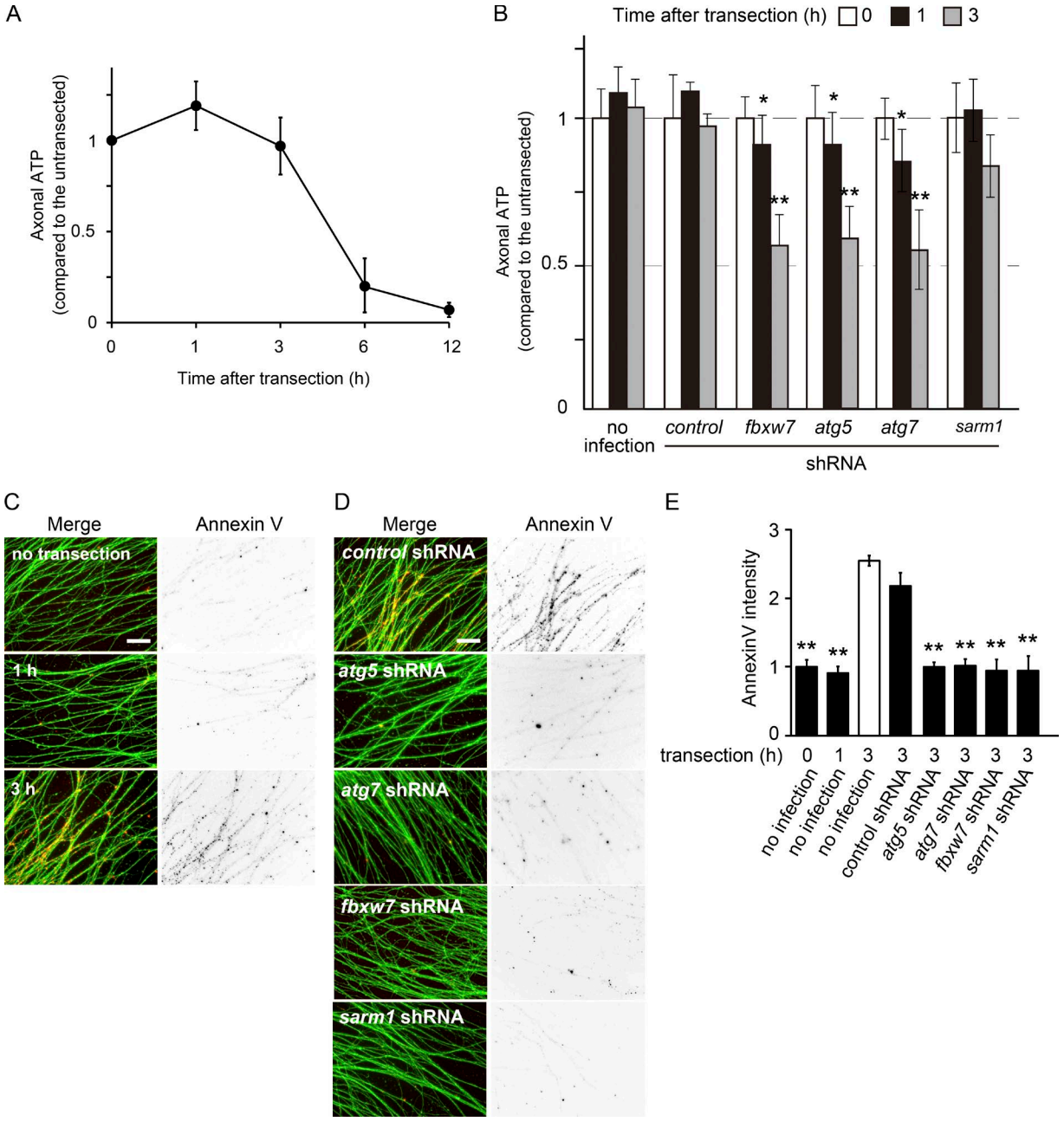

Figure 9. **Inhibition of axonal autophagy disrupts local ATP production and subsequent PS exposure.** (A) ATP levels in the axonal preparation after transection were measured at the indicated time points after transection and are shown as values relative to the level of untransected axons (mean ± SEM, *n* = 5). (B) Inhibition of axonal autophagy disrupts the maintenance of axonal ATP levels at the initiation of Wallerian degeneration. Quantified levels of axonal ATP relative to the level in the control (labeled "no infection, time = 0") are shown (mean ± SEM, *n* = 5). (C) PS exposure on the axons was monitored using the specific probe Alexa Fluor 594–labeled Annexin V. Axons were counterstained with green fluorescent reagent DTAF for visualization. Representative photomicrographs of the fluorescent signal in transected axons at the indicated time points are shown. Bar, 25 µm. (D and E) PS exposure is prevented by the inhibition of axonal autophagy. Representative photomicrographs of the fluorescent signal on transected axons expressing the indicated molecules are shown in D. Bar, 25 µm. Quantified levels of fluorescent intensities for Annexin V normalized to DTAF relative to the control (open bar) are shown in E (mean ± SEM, *n* = 5). Significant differences from the control at each time point (*, P < 0.05; **, P < 0.01) were determined by one-way analysis of variance with Tukey's post-hoc test.

ATG7 (2631; Cell Signaling Technology). HRP-conjugated (Vector Laboratories), Alexa Fluor 565–conjugated, and Alexa Fluor 488–conjugated (Molecular Probes) antibodies were used as secondary antibodies for detection.

DRG explant culture and in vitro Wallerian degeneration

Murine DRG explants dissected from embryonic day 13 C56BL/6J mice were cultured on poly-L-lysine– and laminin-coated 24-well plates in Neuro medium (Miltenyi Biotec) containing 10% FBS and 25 ng/ml NGF (Envigo). After 24 h, the culture medium was changed to Neuro medium supplemented with 2% Neuro-Brew-21 (Miltenyi Biotec), 25 ng/ml NGF, and 1 mM glutamine in addition to a mixture of 1 mM 5′-fluoro-2′-deoxyuridine and 1 mM uridine to remove nonneuronal cells. The in vitro Wallerian degeneration of axons was introduced by removing cell bodies at 10–14 d in vitro using a pipette tip (Wakatsuki et al., 2011, 2015).

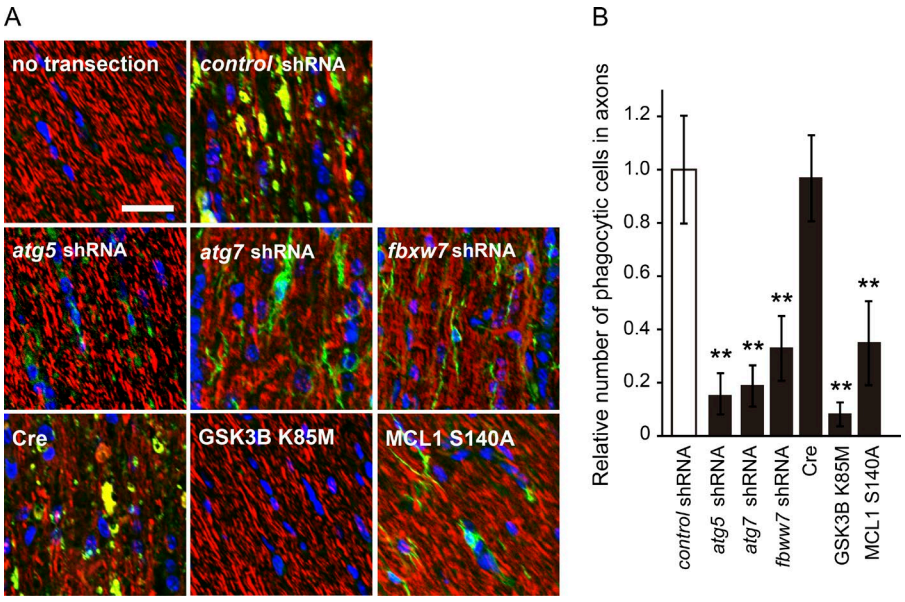

Figure 10. **Inhibition of autophagy in optic nerve axons deteriorates the recruitment of phagocytes to axonal debris.** A unilateral intravitreal injection of adenoviral vector solution for the expression of the indicated molecules in retinal ganglion neurons was performed in adult mice, followed by optic nerve transection 5 d after the injection to induce Wallerian degeneration. The degeneration of the optic nerve (between the eye and optic chiasm) was assessed by immunostaining using antibodies against βIII-tubulin (red) and F4/80 (green) 2 d after axotomy. Nuclei were counterstained with DAPI. Representative photomicrographs for the immunostaining of longitudinal optic nerve sections are shown in A. Bar, 25 µm. Immunofluorescent intensity ratio of the F4/80-stained axonal area to the total axonal area in each condition relative to that of the nontarget control shRNA-expressing condition, representing the relative number of phagocytic cells in axons under each condition, is shown in B (mean ± SEM, $n = 3$). The nontarget control shRNA-expressing condition and Cre-only expression serve as negative controls for the shRNA-mediated down-regulation and overexpression of the indicated molecules, respectively. Significant differences from the control (**, $P < 0.01$) were determined by one-way analysis of variance with Tukey's post-hoc test.

Axonal preparation

To prepare DRG axons, cell culture inserts were coated with poly-L-lysine and laminin at 4°C overnight and placed in a well containing 2 ml of medium with 50 ng/ml NGF in a six-well plate. The inner side of the insert was filled with 1 ml medium. DRG explants (40–50 explants for each condition) were placed within the inserts and cultured as described in DRG explant culture and in vitro Wallerian degeneration. Axon samples were obtained from the bottom surface of the insert and used for biochemical analyses.

Isolation of the mitochondrial fraction

The mitochondrial fraction was isolated from axonal preparations using the mitochondria isolation kit for cultured cells (89874; Thermo Fisher Scientific) according to the manufacturer's protocol. In brief, axonal preparations from each experimental condition were incubated with 200 µl of mitochondria isolation reagent A and homogenized on ice with a micro tissue grinder (357848; Wheaton). Debris was removed by centrifugation at 700 *g* for 10 min at 4°C. The supernatant was further centrifuged at 12,000 *g* for 15 min at 4°C. The supernatant (cytosolic fraction) was collected, and the pellet (mitochondrial fraction) was lysed in RIPA buffer (1% Triton X-100, 0.5% sodium deoxycholate, 0.1% SDS, 150 mM NaCl, and 50 mM Tris-HCl, pH 7.5) containing phosphatase (07574-61; Nacalai Tesque) and protease (25955-11; Nacalai Tesque) inhibitor cocktails.

Immunoblot and immunoprecipitation

Regarding the immunoblot analysis, cultured cells or tissues were homogenized in RIPA buffer containing phosphatase and protease inhibitor cocktails. Equal amounts of protein were separated by SDS-PAGE, followed by immunoblotting. Immunoreactivity was visualized using HRP-conjugated secondary antibodies and a chemiluminescent substrate (Wako Pure Chemical Industries). Chemiluminescent images were captured by LAS4000-mini and quantified using ImageJ software. Scans at multiple exposures were obtained to ensure that the results fell within the linear range of the instrument.

Regarding immunoprecipitation, cells or tissues were lysed in TNE buffer (1% Triton X-100, 100 mM NaCl, and 20 mM Tris-HCl, pH 7.5) containing protease inhibitor cocktail. After centrifugation at 15,000 *g* for 30 min, the supernatant was incubated at 4°C overnight with the primary antibody. After being incubated with protein A-coupled Dynabeads, proteins were eluted by boiling for 5 min in Laemmli sample buffer and analyzed by immunoblotting.

Plasmid construction and mutagenesis

The coding region of MCL1 was amplified by PCR using LA-taq (Takara Bio Inc.), the full-length coding region of the MCL1 cDNA (GenBank accession number NM_008562), and cloned into the indicated expression plasmids. The integrity of each clone was confirmed by sequencing. Regarding detection, a His tag or MYC tag was added to the C terminus of MCL1 or GSK3B. pcDNA3-FBXW7 was provided by K. Nakayama (Kyushu University, Fukuoka, Japan; Yada et al., 2004). MCL1 mutants (S140A, S140D, K117R, K175/178R, and K117/175/178R) were generated by PCR-mediated site-directed mutagenesis, and an HA tag was added at their C termini. The constitutively active form of AKT (myrAKT-HA) was generated by adding a myristoylation site derived from murine Src tyrosine kinase to the N-terminal end of the AKT-HA construct.

Viral vectors and infection

A pAxCALNLwtit2 cosmid vector (Takara Bio Inc.) was used for all experiments involving adenovirus-mediated gene expression to achieve the Cre recombinase-mediated activation of the genes of interest and EGFP to visualize transgene activation in live cells by way of an internal ribosome entry site. cDNAs for myristoylated AKT-HA, GSK3B-MYC, GSK3B-MYC S9A, GSK3B-MYC K85M, MCL1-His, MCL1-His S140A, and MCL1-His S140D were constructed as described above. A recombinant adenovirus was generated using the Takara adenovirus expression kit (Takara Bio Inc.) according to the manufacturer's instructions. The purification and concentration of adenoviral vectors was achieved and measured by two rounds of cesium chloride density gradient centrifugation and Centricon

Centrifugal Filter Devices (EMD Millipore), respectively, according to the manufacturers' instructions. Viral titers were measured with a plaque-forming assay in HEK293 cells.

In experiments using lentiviral vectors, control and specific shRNAs in the pLKO.1 puromycin-resistant lentiviral vector were purchased from Sigma-Aldrich. The following clones were used: FBXW7 #1, TRCN0000373989; FBXW7 #2, TRCN0000365828; MULE #1, TRCN0000092556; MULE #2, TRCN0000092555; MCL1 #1, TRCN0000273764; MCL1 #2, TRCN0000004693; ATG5 #1, TRCN0000099432; ATG5 #2, TRCN0000375819; ATG7 #1, TRCN0000375444; ATG7 #2, TRCN0000305991; SARM1, TRCN0000193408; and nontarget control, SHC002. Constructs for MCL1-HA, FLAG-BCL2, and FLAG-BCLW were generated as described earlier. Lentiviral packaging was performed using HEK293FT cells, as previously described (Araki et al., 2004).

Quantitative RT-PCR

Total RNA was extracted from cultured DRG neurons or Neuro-2a cells using the RNeasy MiniKit (QIAGEN). Real-time quantitative RT-PCR was performed as previously described (Wakatsuki et al., 2011, 2015) using the Applied Biosystems Prism model 7300 sequence detection instrument and a standard SYBR green detection protocol. The sequences of the PCR primers using the SYBR green method are as follows: glyceraldehyde-3-phosphate dehydrogenase (GAPDH) forward, 5′-CCCCCA ATGTATCCGTTGTG-3′, and reverse, 5′-TAGCCCAGGATGCCCTTT AGT-3′; ATG5 forward, 5′-TGTGCTTCGAGATGTGTGGTT-3′, and reverse, 5′-GTCAAATAGCTGACTCTTGGCAA-3′; ATG7 forward, 5′-GTTCGCCCCCTTTAATAGTGC-3′, and reverse, 5′-TGAACTCCA ACGTCAAGCGG-3′; MCL1 forward, 5′-AAAGGCGGCTGCATA AGTC-3′, and reverse, 5′-TGGCGGTATAGGTCGTCCTC-3′; FBXW7 forward, 5′-GTTCCGCTGCCTAATCTTCCT-3′, and reverse, 5′-CCC TTCAGGGATTCTGTGCC-3′; and MULE forward, 5′-AGAAAGCGG ATGGTACTGCTA-3′, and reverse, 5′-AACGACCTGCTGATTAGG CTC-3′. The samples were run in duplicate. The expression level for each sample of interest was normalized to GAPDH.

Microscopy image acquisition

In immunohistochemical analyses, mice were fixed with 4% PFA in PBS. The optic nerves were dissected to analyze neurofilament M and βIII-tubulin immunoreactivity. Coronal sections (thickness of 20 µm) were cut on a cryostat (Microm HM550; ZEISS). In the immunocytochemical analysis of the axons of cultured DRG neurons, DRG neurons were fixed with 4% PFA in PBS and permeabilized with 0.2% Triton X-100 in PBS. Incubation with primary antibody was performed at 4°C overnight, followed by secondary antibody at RT for 1 h. Specimens were mounted in Vectashield mounting medium (Vector Laboratories). Immunofluorescence was observed under an inverted microscope (DMI 6000B; Leica Biosystems) and analyzed using LAS AF software (version 3.2; Leica Biosystems). Confocal microscope images were observed under a confocal microscope (FluoView FV1000 IX81; Olympus) and analyzed using FluoView FV10-ASW 3.1 software (Olympus). Images were taken with a constant exposure time between all the conditions of the same experiment and were processed using Photoshop software (Adobe Systems).

Intravitreal injection of adenoviral vectors, optic nerve transection, and histological analysis

Mice were anesthetized using an intraperitoneal injection of avertin. An intravitreal injection of adenoviral vector solution (1 µl; $5 \times 10^8 \sim 10^9$ pfu) was performed unilaterally for the expression of genes of interest in retinal ganglion cells. 7 d after the injection, the Wallerian degeneration of optic nerve fibers was introduced by enucleation. 5 d after surgery, animals were perfused with 4% PFA in PBS for immunohistochemical analyses or killed to collect the injured optic segment and contralateral control for the immunoblot analysis.

5 d after surgery, mice were anesthetized by an intraperitoneal injection of avertin and perfusion fixed transcardially with 2% PFA and 2.5% glutaraldehyde in PBS. Fixed optic nerves were removed and embedded in 3% agarose in PBS. Transverse sections (thickness of 100 µm) were prepared using a Microslicer (DTK-3000; Dosaka), and sections of the location 2 mm distal to the transected site were selected under microscopic observation. The selected sections were rinsed, osmicated, dehydrated, and embedded in epoxy resin. Ultrathin sections were prepared, stained with lead citrate and uranyl acetate, and observed under a transmission electron microscope (Tecnai Spirit; Thermo Fisher Scientific). To assess the delayed Wallerian degeneration effect by the inhibition of the GSK3B–MCL1 pathway, healthy axons preserved in optic nerves expressing the indicated molecules (n = 5 for each condition) were counted. All axons in a 10 × 10-µm square field were counted for quantification in each sample. Double-membrane vacuole-like structures in axons expressing the indicated molecules (n = 5 for each condition) were counted to assess the suppressive effects of the inhibition of the GSK3B–MCL1 pathway on autophagosome formation. The number of double-membrane vacuole-like structures in axons in a 10 × 10-µm square field was counted for each sample.

Quantification of in vitro Wallerian degeneration

To quantify axonal degeneration in a culture (Wakatsuki et al., 2011), captured images of axons in a culture were binarized such that pixels corresponding to axons were converted to black and all other regions were converted to white. Continuous stretches of black pixels larger than 10,000 were designated as "healthy axons," and all others as "degenerated axons." The number of pixels for each type of axon was counted. To detect degenerated axons, we used the particle analyzer module of ImageJ software with plug-ins FeatureJ and ImageScience. The axon degeneration index was defined as the ratio of the degenerated axon pixel number to the total (healthy plus degenerated) axon pixel number. Three or four nonoverlapping images per explant were randomly collected. More than five explants were examined for each experimental condition.

Evaluation of PS exposure

PS exposure on transected axons of cultured DRG neurons was evaluated using Alexa Fluor 594–labeled Annexin V (A13203; Thermo Fisher Scientific). Axons were costained with 5-([4,6-dichlorotriazinyl]amino)fluorescein (DTAF; D-16; Thermo Fisher Scientific) for visualization. Three nonoverlapping images per explant were randomly collected. More than five explants were examined for each experimental condition. To evaluate PS exposure on transected axons, the fluorescent intensities of each image were measured using ImageJ software (National Institutes of Health). Quantified levels of fluorescent intensities for PS normalized to DTAF were averaged and compared with the control.

Measurement of axonal ATP levels

An axon preparation was lysed and subjected to ATP measurements with the ATPlite Luminescence Assay System (6016943; Perkin-Elmer) according to the manufacturer's instructions. Protein concentrations in each extract were determined using the BCA assay. Results are presented as ATP levels relative to the control normalized by protein concentrations.

Assessment of mitochondrial membrane potential

The mitochondrial membrane potential (MMP) was assessed using JC-1 (5,5′,6,6'-tetrachloro-1,1′,3,3′-tetraethylbenzimidazolyl-carbocyanine

iodide; T3168; Thermo Fisher Scientific), which forms a monomer at low MMP and an aggregate at higher MMP, or tetramethylrhodamine methyl ester (TMRM), which is accumulated in mitochondria with normal MMP. Cultures of DRG neurons were incubated with 1 µg/ml JC-1 at 37°C for 30 min and washed three times with culture medium. Images were taken using a DMI 6000B (excitation, λ = 488 nm; emission, λ = 530 and 590 nm for green monomers and red aggregates, respectively). Fluorescence intensity of the red/green ratio was determined semiquantitatively with ImageJ. For TMRM-based measurement, cultured DRG neurons were incubated with 50 nM TMRM at 37°C for 30 min. Images were taken using a DMI 6000B. Image analysis was performed with ImageJ to calculate TMRM fluorescence obtained from neurite area in control and after injury (Scaduto and Grotyohann, 1999).

Statistical analysis

Results are expressed as mean ± SEM. Differences between groups were examined for significance using one-way analysis of variance with Tukey's post hoc test.

Online supplemental material

Fig. S1 demonstrates that FBXW7 ubiquitin ligase regulates MCL1 stability. Fig. S2 shows that the GSK3B–MCL1 pathway induces axonal autophagy and axonal degeneration after transection. Fig. S3 demonstrates the molecular mechanisms of axonal autophagy. Fig. S4 demonstrates that the mitochondrial function is not affected by inhibition of *fbxw7* expression in axons. Fig. S5 shows the schematic representation of the GSK3B–MCL1 signaling mechanism–dependent induction of axonal autophagy.

Acknowledgments

We thank Drs. Sumiko Kiryu-Seo, Noriyuki Matsuda, and Gen Matsumoto for their technical advice.

This work was supported in part by a Grant-in-Aid for Scientific Research on Innovative Areas ("Brain Environment") from the Ministry of Education, Culture, Sports, Science and Technology (S. Wakatsuki); a Grant-in-Aid for Scientific Research from the Japan Society for the Promotion of Science (S. Wakatsuki); Intramural Research Grant for Neurological and Psychiatric Disorders of National Center of Neurology and Psychiatry (T. Araki); grants from Takeda Science Foundation (S. Wakatsuki and T. Araki), and Pfizer academic contributions (T. Araki).

The authors declare no competing financial interests.

Submitted: 3 June 2016
Revised: 25 October 2016
Accepted: 22 December 2016

References

Araki, T., Y. Sasaki, and J. Milbrandt. 2004. Increased nuclear NAD biosynthesis and SIRT1 activation prevent axonal degeneration. *Science.* 305:1010–1013. http://dx.doi.org/10.1126/science.1098014

Conforti, L., J. Gilley, and M.P. Coleman. 2014. Wallerian degeneration: An emerging axon death pathway linking injury and disease. *Nat. Rev. Neurosci.* 15:394–409. http://dx.doi.org/10.1038/nrn3680

Daleke, D.L., and J.V. Lyles. 2000. Identification and purification of aminophospholipid flippases. *Biochim. Biophys. Acta.* 1486:108–127. http://dx.doi.org/10.1016/S1388-1981(00)00052-4

Ekholm-Reed, S., M.S. Goldberg, M.G. Schlossmacher, and S.I. Reed. 2013. Parkin-dependent degradation of the F-box protein Fbw7β promotes neuronal survival in response to oxidative stress by stabilizing Mcl-1. *Mol. Cell. Biol.* 33:3627–3643. http://dx.doi.org/10.1128/MCB.00535-13

Elliott, J.I., A. Surprenant, F.M. Marelli-Berg, J.C. Cooper, R.L. Cassady-Cain, C. Wooding, K. Linton, D.R. Alexander, and C.F. Higgins. 2005. Membrane phosphatidylserine distribution as a non-apoptotic signalling mechanism in lymphocytes. *Nat. Cell Biol.* 7:808–816. http://dx.doi.org/10.1038/ncb1279

Gerdts, J., D.W. Summers, J. Milbrandt, and A. DiAntonio. 2016. Axon self-destruction: New links among SARM1, MAPKs, and NAD+ metabolism. *Neuron.* 89:449–460. http://dx.doi.org/10.1016/j.neuron.2015.12.023

Germain, M., A.P. Nguyen, J.N. Le Grand, N. Arbour, J.L. Vanderluit, D.S. Park, J.T. Opferman, and R.S. Slack. 2011. MCL-1 is a stress sensor that regulates autophagy in a developmentally regulated manner. *EMBO J.* 30:395–407. http://dx.doi.org/10.1038/emboj.2010.327

He, C., and B. Levine. 2010. The Beclin 1 interactome. *Curr. Opin. Cell Biol.* 22:140–149. http://dx.doi.org/10.1016/j.ceb.2010.01.001

Inuzuka, H., S. Shaik, I. Onoyama, D. Gao, A. Tseng, R.S. Maser, B. Zhai, L. Wan, A. Gutierrez, A.W. Lau, et al. 2011. SCF(FBW7) regulates cellular apoptosis by targeting MCL1 for ubiquitylation and destruction. *Nature.* 471:104–109. http://dx.doi.org/10.1038/nature09732

Ivatt, R.M., A. Sanchez-Martinez, V.K. Godena, S. Brown, E. Ziviani, and A.J. Whitworth. 2014. Genome-wide RNAi screen identifies the Parkinson disease GWAS risk locus SREBF1 as a regulator of mitophagy. *Proc. Natl. Acad. Sci. USA.* 111:8494–8499. http://dx.doi.org/10.1073/pnas.1321207111

Kang, R., H.J. Zeh, M.T. Lotze, and D. Tang. 2011. The Beclin 1 network regulates autophagy and apoptosis. *Cell Death Differ.* 18:571–580. http://dx.doi.org/10.1038/cdd.2010.191

Komatsu, M., S. Waguri, T. Ueno, J. Iwata, S. Murata, I. Tanida, J. Ezaki, N. Mizushima, Y. Ohsumi, Y. Uchiyama, et al. 2005. Impairment of starvation-induced and constitutive autophagy in Atg7-deficient mice. *J. Cell Biol.* 169:425–434. http://dx.doi.org/10.1083/jcb.200412022

Komatsu, M., Q.J. Wang, G.R. Holstein, V.L. Friedrich Jr., J. Iwata, E. Kominami, B.T. Chait, K. Tanaka, and Z. Yue. 2007. Essential role for autophagy protein Atg7 in the maintenance of axonal homeostasis and the prevention of axonal degeneration. *Proc. Natl. Acad. Sci. USA.* 104:14489–14494. http://dx.doi.org/10.1073/pnas.0701311104

Kuma, A., M. Hatano, M. Matsui, A. Yamamoto, H. Nakaya, T. Yoshimori, Y. Ohsumi, T. Tokuhisa, and N. Mizushima. 2004. The role of autophagy during the early neonatal starvation period. *Nature.* 432:1032–1036. http://dx.doi.org/10.1038/nature03029

Lum, J.J., R.J. DeBerardinis, and C.B. Thompson. 2005. Autophagy in metazoans: Cell survival in the land of plenty. *Nat. Rev. Mol. Cell Biol.* 6:439–448. http://dx.doi.org/10.1038/nrm1660

Maday, S., and E.L. Holzbaur. 2016. Compartment-specific regulation of autophagy in primary neurons. *J. Neurosci.* 36:5933–5945. http://dx.doi.org/10.1523/JNEUROSCI.4401-15.2016

Maurer, U., C. Charvet, A.S. Wagman, E. Dejardin, and D.R. Green. 2006. Glycogen synthase kinase-3 regulates mitochondrial outer membrane permeabilization and apoptosis by destabilization of MCL-1. *Mol. Cell.* 21:749–760. http://dx.doi.org/10.1016/j.molcel.2006.02.009

Mellén, M.A., E.J. de la Rosa, and P. Boya. 2008. The autophagic machinery is necessary for removal of cell corpses from the developing retinal neuroepithelium. *Cell Death Differ.* 15:1279–1290. http://dx.doi.org/10.1038/cdd.2008.40

Mizushima, N., A. Yamamoto, M. Hatano, Y. Kobayashi, Y. Kabeya, K. Suzuki, T. Tokuhisa, Y. Ohsumi, and T. Yoshimori. 2001. Dissection of autophagosome formation using Apg5-deficient mouse embryonic stem cells. *J. Cell Biol.* 152:657–668. http://dx.doi.org/10.1083/jcb.152.4.657

Mizushima, N., A. Yamamoto, M. Matsui, T. Yoshimori, and Y. Ohsumi. 2004. In vivo analysis of autophagy in response to nutrient starvation using transgenic mice expressing a fluorescent autophagosome marker. *Mol. Biol. Cell.* 15:1101–1111. http://dx.doi.org/10.1091/mbc.E03-09-0704

Mizushima, N., T. Yoshimori, and B. Levine. 2010. Methods in mammalian autophagy research. *Cell.* 140:313–326. http://dx.doi.org/10.1016/j.cell.2010.01.028

Nishida, Y., S. Arakawa, K. Fujitani, H. Yamaguchi, T. Mizuta, T. Kanaseki, M. Komatsu, K. Otsu, Y. Tsujimoto, and S. Shimizu. 2009. Discovery of Atg5/Atg7-independent alternative macroautophagy. *Nature.* 461:654–658. http://dx.doi.org/10.1038/nature08455

Osterloh, J.M., J. Yang, T.M. Rooney, A.N. Fox, R. Adalbert, E.H. Powell, A.E. Sheehan, M.A. Avery, R. Hackett, M.A. Logan, et al. 2012. dSarm/Sarm1 is required for activation of an injury-induced axon death pathway. *Science.* 337:481–484. http://dx.doi.org/10.1126/science.1223899

Qu, X., Z. Zou, Q. Sun, K. Luby-Phelps, P. Cheng, R.N. Hogan, C. Gilpin, and B. Levine. 2007. Autophagy gene-dependent clearance of apoptotic cells during embryonic development. *Cell.* 128:931–946. http://dx.doi.org/10.1016/j.cell.2006.12.044

Ravichandran, K.S. 2011. Beginnings of a good apoptotic meal: The find-me and eat-me signaling pathways. *Immunity.* 35:445–455. http://dx.doi.org/10.1016/j.immuni.2011.09.004

Scaduto, R.C. Jr., and L.W. Grotyohann. 1999. Measurement of mitochondrial membrane potential using fluorescent rhodamine derivatives. *Biophys. J.* 76:469–477. http://dx.doi.org/10.1016/S0006-3495(99)77214-0

Schoenmann, Z., E. Assa-Kunik, S. Tiomny, A. Minis, L. Haklai-Topper, E. Arama, and A. Yaron. 2010. Axonal degeneration is regulated by the apoptotic machinery or a NAD+-sensitive pathway in insects and mammals. *J. Neurosci.* 30:6375–6386. http://dx.doi.org/10.1523/JNEUROSCI.0922-10.2010

Shen, H.M., and N. Mizushima. 2014. At the end of the autophagic road: An emerging understanding of lysosomal functions in autophagy. *Trends Biochem. Sci.* 39:61–71. http://dx.doi.org/10.1016/j.tibs.2013.12.001

Shin, J.E., B.R. Miller, E. Babetto, Y. Cho, Y. Sasaki, S. Qayum, E.V. Russler, V. Cavalli, J. Milbrandt, and A. DiAntonio. 2012. SCG10 is a JNK target in the axonal degeneration pathway. *Proc. Natl. Acad. Sci. USA.* 109:E3696–E3705. http://dx.doi.org/10.1073/pnas.1216204109

Suzuki, J., D.P. Denning, E. Imanishi, H.R. Horvitz, and S. Nagata. 2013. Xk-related protein 8 and CED-8 promote phosphatidylserine exposure in apoptotic cells. *Science.* 341:403–406. http://dx.doi.org/10.1126/science.1236758

Tai, W.T., C.W. Shiau, H.L. Chen, C.Y. Liu, C.S. Lin, A.L. Cheng, P.J. Chen, and K.F. Chen. 2013. Mcl-1-dependent activation of Beclin 1 mediates autophagic cell death induced by sorafenib and SC-59 in hepatocellular carcinoma cells. *Cell Death Dis.* 4:e485. http://dx.doi.org/10.1038/cddis.2013.18

van Delft, M.F., A.H. Wei, K.D. Mason, C.J. Vandenberg, L. Chen, P.E. Czabotar, S.N. Willis, C.L. Scott, C.L. Day, S. Cory, et al. 2006. The BH3 mimetic ABT-737 targets selective Bcl-2 proteins and efficiently induces apoptosis via Bak/Bax if Mcl-1 is neutralized. *Cancer Cell.* 10:389–399. http://dx.doi.org/10.1016/j.ccr.2006.08.027

Wakatsuki, S., F. Saitoh, and T. Araki. 2011. ZNRF1 promotes Wallerian degeneration by degrading AKT to induce GSK3B-dependent CRMP2 phosphorylation. *Nat. Cell Biol.* 13:1415–1423. http://dx.doi.org/10.1038/ncb2373

Wakatsuki, S., A. Furuno, M. Ohshima, and T. Araki. 2015. Oxidative stress-dependent phosphorylation activates ZNRF1 to induce neuronal/axonal degeneration. *J. Cell Biol.* 211:881–896. http://dx.doi.org/10.1083/jcb.201506102

Wang, J., Q. Zhai, Y. Chen, E. Lin, W. Gu, M.W. McBurney, and Z. He. 2005. A local mechanism mediates NAD-dependent protection of axon degeneration. *J. Cell Biol.* 170:349–355. http://dx.doi.org/10.1083/jcb.200504028

Wang, J.T., Z.A. Medress, and B.A. Barres. 2012. Axon degeneration: Molecular mechanisms of a self-destruction pathway. *J. Cell Biol.* 196:7–18. http://dx.doi.org/10.1083/jcb.201108111

Wertz, I.E., S. Kusam, C. Lam, T. Okamoto, W. Sandoval, D.J. Anderson, E. Helgason, J.A. Ernst, M. Eby, J. Liu, et al. 2011. Sensitivity to antitubulin chemotherapeutics is regulated by MCL1 and FBW7. *Nature.* 471:110–114. http://dx.doi.org/10.1038/nature09779

Wong, Y.C., and E.L. Holzbaur. 2015. Autophagosome dynamics in neurodegeneration at a glance. *J. Cell Sci.* 128:1259–1267. http://dx.doi.org/10.1242/jcs.161216

Xingyong, C., S. Xicui, S. Huanxing, O. Jingsong, H. Yi, Z. Xu, H. Ruxun, and P. Zhong. 2013. Upregulation of myeloid cell leukemia-1 potentially modulates beclin-1-dependent autophagy in ischemic stroke in rats. *BMC Neurosci.* 14:56. http://dx.doi.org/10.1186/1471-2202-14-56

Xiong, X., Y. Hao, K. Sun, J. Li, X. Li, B. Mishra, P. Soppina, C. Wu, R.I. Hume, and C.A. Collins. 2012. The Highwire ubiquitin ligase promotes axonal degeneration by tuning levels of Nmnat protein. *PLoS Biol.* 10:e1001440. http://dx.doi.org/10.1371/journal.pbio.1001440

Yada, M., S. Hatakeyama, T. Kamura, M. Nishiyama, R. Tsunematsu, H. Imaki, N. Ishida, F. Okumura, K. Nakayama, and K.I. Nakayama. 2004. Phosphorylation-dependent degradation of c-Myc is mediated by the F-box protein Fbw7. *EMBO J.* 23:2116–2125. http://dx.doi.org/10.1038/sj.emboj.7600217

Yamamoto, A., and Z. Yue. 2014. Autophagy and its normal and pathogenic states in the brain. *Annu. Rev. Neurosci.* 37:55–78. http://dx.doi.org/10.1146/annurev-neuro-071013-014149

Yang, Z., and D.J. Klionsky. 2010. Mammalian autophagy: Core molecular machinery and signaling regulation. *Curr. Opin. Cell Biol.* 22:124–131. http://dx.doi.org/10.1016/j.ceb.2009.11.014

Yang, J., Z. Wu, N. Renier, D.J. Simon, K. Uryu, D.S. Park, P.A. Greer, C. Tournier, R.J. Davis, and M. Tessier-Lavigne. 2015. Pathological axonal death through a MAPK cascade that triggers a local energy deficit. *Cell.* 160:161–176. http://dx.doi.org/10.1016/j.cell.2014.11.053

Yang, Y., M. Coleman, L. Zhang, X. Zheng, and Z. Yue. 2013. Autophagy in axonal and dendritic degeneration. *Trends Neurosci.* 36:418–428. http://dx.doi.org/10.1016/j.tins.2013.04.001

Zhong, Q., W. Gao, F. Du, and X. Wang. 2005. Mule/ARF-BP1, a BH3-only E3 ubiquitin ligase, catalyzes the polyubiquitination of Mcl-1 and regulates apoptosis. *Cell.* 121:1085–1095. http://dx.doi.org/10.1016/j.cell.2005.06.009